AN ABSTRACT OF THE THESIS OF

Elmer Harvey Elwin (Name) for the Master of Science (Degree)

in Civil Engineering (Major) presented on May 8, 1969 (Date)

Title: Entering Streamflow Effects on Currents of a Density Stratified Model Reservoir

Redacted for Privacy

Abstract approved: Larry S. Slotta

The effect of entering streamflow on currents of a density stratified reservoir has been studied in a laboratory model to provide insight into the prediction, control, and maintenance of quality water discharge from a thermally stratified reservoir. Twenty experiments were performed using various concentrations of a sodium chloride solution to provide a linear density stratification and using photographic techniques to provide velocity measurements of the flow field. General flow patterns are described and graphical presentation of dimensionless parameters quantitatively relate the existence, location, and magnitude of model internal density currents to entering streamflow characteristics. The applicability of the results to a prototype reservoir is discussed.

Entering Streamflow Effects on Currents of a Density Stratified Model Reservoir

by

Elmer Harvey Elwin

A THESIS

submitted to

Oregon State University

in partial fulfillment of
the requirements for the
degree of

Master of Science

June 1969

APPROVED:

Redacted for Privacy

Associate Professor of Civil Engineering
in charge of major

Redacted for Privacy

Head of Department of Civil Engineering

Redacted for Privacy

Dean of Graduate School

Date thesis is presented May 8, 1969

Typed by Velda D. Mullins for Elmer Harvey Elwin

ACKNOWLEDGMENT

The author wishes to acknowledge the financial support for the research herein provided by the Grant W 00983-02 from the Federal Water Pollution Control Administration, U.S. Department of Interior, entitled "Stratified Reservoir Currents." He further wishes to express his deepest gratitude to Dr. Larry S. Slotta, his major professor, for the guidance and support received. Thanks are also due to the many people who contributed to the author's better understanding of this project; particularly, T. Spurkland and Dr. R. W. Filmer. Special thanks to my wife, Carlann, for her patience and aid in the preparation of this manuscript.

TABLE OF CONTENTS

LIST OF FIGURES

Entering Streamflow Effects on Currents of a Density Stratified Model Reservoir

I. INTRODUCTION

In recent years increasing populations with increasing demands of water for municipal and agricultural uses, together with rapidly expanding industrial needs are putting increasing pressure on man's most important natural resource--water. This pressure has been periodically eased by the authorization and construction of an increasing number of impounding reservoirs, however the total supply of quality water eventually will be limited, and man must learn to use his supplies efficiently.

In order to use a water supply more efficiently, man must be concerned with water quality because the value of a quantity of water is a function of its quality. If man could sort his water supply on the basis of quality, maximum efficiency in reservoir management could be achieved. For example, if man knew how to predict and control the quality and movement of water in a reservoir the most potable water could be drawn off for domestic needs, the coolest water used for industrial cooling, the warmest water saved for recreation, and the life of impoundments lengthened by using sediment laden water for irrigation. The quality of conservation flows could be controlled for maximum benefits to fish and

wildlife, and short term polluted flows could be passed through water supplies with a minimum of pollution. Thus, efficient reservoir management is related to the quality and movement of water behind a reservoir.

1. Effect of Impoundment on Quality.

Water quality characteristics may be grouped into three categories: physical characteristics--temperature and turbidity; chemical characteristics--dissolved oxygen, nitrogen, dissolved minerals, and other substances; and biological characteristics--biological oxygen demand, coliform count, and algae count.

Impoundment is among the many things that effect water quality. When a flowing river is dammed and becomes an impoundment, two major changes occur that have a marked effect on water quality. First, an impoundment greatly increases the time required for water to travel the distance from the headwaters to the dam's discharge location. Second, stratification due to density variation in an impoundment changes the characteristics of the water discharged at a given location from what they originally were when the stream was flowing free. Some of the important effects are: a reduction in turbidity; a variation in temperature and dissolved oxygen; and, an increase in algae growth, dissolved solids, nitrogen and phosphorous.

The most important factor in the variation of water quality within a reservoir or lake is a variation in its density. Although density variations or stratification may occasionally be due to chemicals, wastes, or suspended sediments, temperature is analogous in creating density variations. It is well recognized that lakes and reservoirs in the temperate zone undergo a complex seasonal variation in temperature. Typical seasonal and spatial variations of temperature in a deep, temperate climate lake are shown in Figure 1.

During winter and at the beginning of spring a lake is virtually at a uniform temperature throughout its depth, and is essentially homogeneous. During early summer with the coming of warmer weather a definite temperature profile develops as water near the surface absorbs more energy and is, therefore, warmed faster. Through the summer, heat is absorbed at the surface and mixed downward, largely by wind action with the surface temperature only changing slightly. In late summer a reservoir will have obtained maximum stratification. After this time, as the weather cools, the surface temperature begins to fall creating an unstable condition. Surface water as it cools is more dense than the water beneath it. Overturning occurs and the mixing results eventually in an isothermic condition. The cylical variation of temperature is controlled by various inputs and outputs of energy; solar

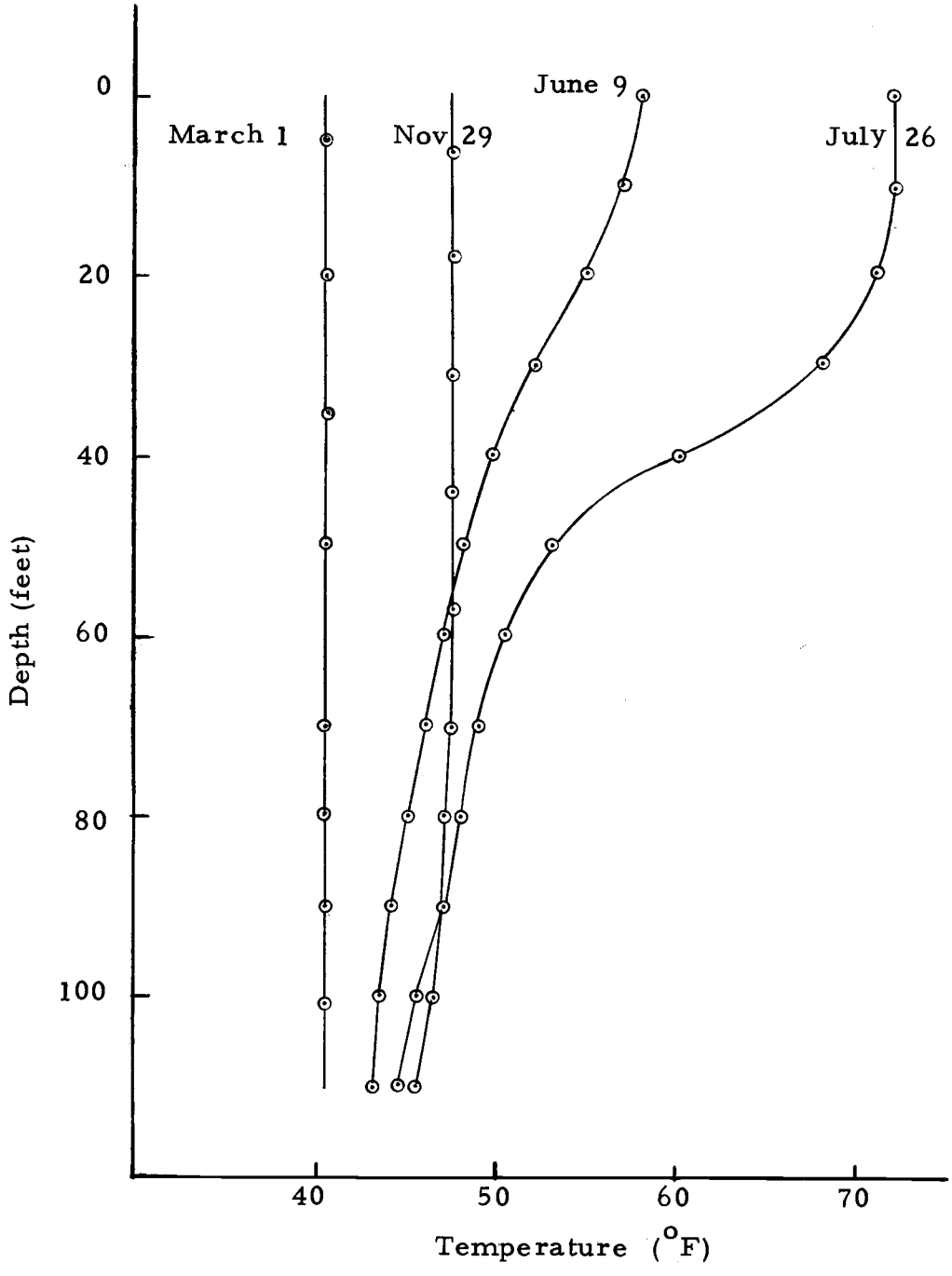

Figure 1. Temperature profiles of the west basin of Horn Lake, B. C., during 1960. (Clay and Fahlman, 1962)

radiation; the convection of heat into and out of the reservoir; evaporation; and back radiation. Analytical and experimental work has been done in an attempt to predict thermal stratification of lakes and reservoirs by Dake and Harleman (9), and an actual method of prediction has been used with good results on Hungry Horse reservoir by Ross and MacDonald (25).

The zone of steep gradient which joins the upper mixed layer (epilimnion) to the cooler body of water below (hypolimnion) is generally referred to as the metalimnion of thermocline. The definitions are illustrated in Figure 2.

Stratification is most important in determining water quality in reservoirs. It may influence water quality through a direct relationship between density and physical or chemical quality parameters, or it may influence water quality by controlling movement of water in the reservoir. The movement of water in the reservoir determines detention time and has an influence on biological quality parameters.

2. Internal Currents

The variations of fluid density in a thermally stratified reservoir give rise to internal flow patterns which may differ entirely from those encountered in homogenous fluids under similar boundary conditions. These flow patterns are known as internal

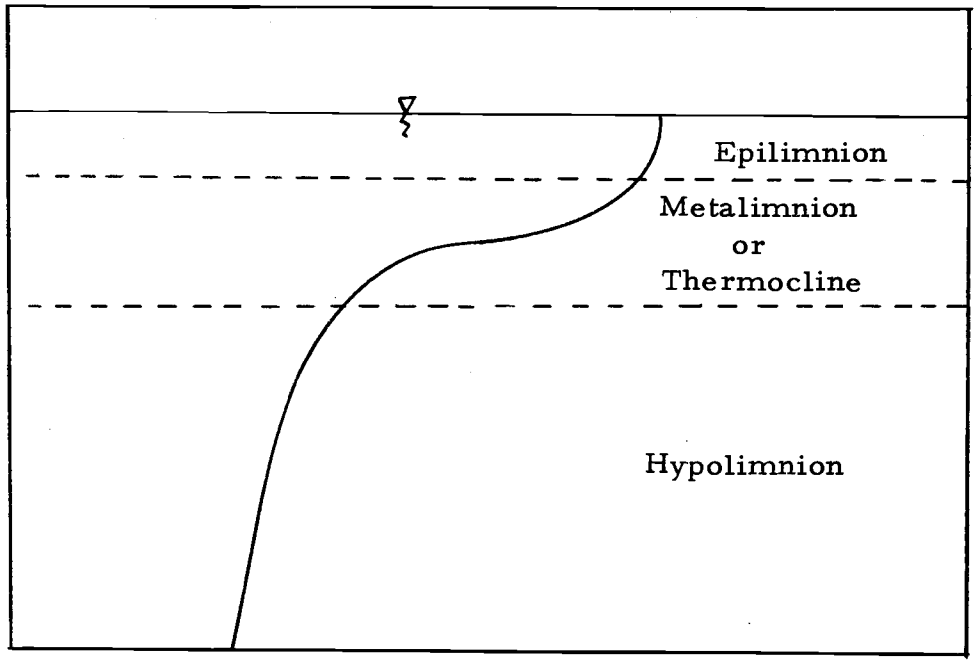

Figure 2. Definition of regions associated with thermal stratification.

density currents.

Internal density currents, although extremely apparent in the flow regime of a reservoir, are not restricted only to reservoirs. A density current may be the gravitationally induced flow of any fluid which is slightly different in density than its surroundings, and the density difference may be due to chemicals, temperature, or suspensions. Interesting cases of density currents may be found in oceanography, hydrology, meteorology, or geology. Ellison and Turner (11) have reviewed some of the situations in nature where nonsuspension density currents occur.

These include the flow of katabatic winds in the atmosphere; the flow of cold water on the ocean floor from arctic to equatorial regions; and the flow of methane fluids along the roof of a mine gallery. Also, Middleton (21) has studied the existence of the turbidity or suspension type density currents over the ocean floor as a means of forming graded offshore beds. Thus this reservoir study has its analog in oceanographic and meteorological investigations.

Density currents in reservoirs are classified by Churchill (6) as three types--overflows, interflows, and underflows. Although Churchill describes these three types of density currents only in terms of the position of the inflowing streams of water, it is recognized that the same types of density currents may be created also by withdrawal from a reservoir. Regardless of whether internal density currents are created by withdrawal or by inflow or by a combination of withdrawal and inflow, they are important to water quality as shown in the following cases.

Density currents exist and cause some unique effects in the Watts Bar reservoir of the TVA system that furnishes the water supply for Harriman, Tennessee (6). The Harriman water plant intake is located approximately one mile from the upper limit of the backwater on the Emory River arm of the pool and about 13 miles above the junction of the Emory and Clinch

arms of the pool. During the winter months, or whenever fairly high flows from the Emory River headwaters exist, the direction of the streamflow for the entire cross section of the pool is downstream from the waterworks. During the summer months, however, when low velocities normally exist, cold water released at Norris Dam into the Clinch River can run upstream in the warmer waters of the Emory arm. As the cold Clinch River water flows up the Emory arm of the pool as a density current, it flows past the Harriman sewer outlets and also past the outfall from a large paper mill. Sewage and mill waste are discharged into the cold water current and are carried by it upstream to the intake of the Harriman water plant, located about one and one-half miles above the paper mill outfall. No one had earlier realized that density currents would extend upstream into the Emory arm of the pool, a distance of 13 miles, but now that they are recognized, the situation has been corrected by using a variable level outfall for the sewage and mill waste.

Turbid density currents have been recognized in America since 1914, when they were reported as having occurred several times in Zuni Reservoir, New Mexico. Most commonly they occur as streamflow entering clear lakes and reservoirs loaded with sediment as a result of floods, but may also result from subsurface landslides. In an early paper, Bell (2) discusses

turbidity currents in connection with the sedimentation of Lake Mead. He says the turbidity currents were transporting fine sediments into lower Lake Mead at a rate that will occupy one percent of the original spillway crest capacity each 8.2 years. It is also estimated that by encouraging withdrawal from this turbidity current, much of the sediment may be discharged before it has settled, and that the useful like of Lake Mead could be lengthened by 20 percent in this manner.

In order to increase the production of Pacific salmon the Canadian Department of Fisheries has established a fish hatchery on the Big Qualicum River in British Columbia. In order to improve conditions for the fishery, it has been considered desirable that a uniform flow of approximately 200 cfs be maintained during the spawning period from late summer to mid-winter. Since the Big Qualicum is at its extreme low flow during the late summer and early fall, a reservoir was established. It was found that under controlled flow conditions, the increased summer minimum flows masked the cooling influence of groundwater sources downstream from the reservoir. In order to keep the stream temperature of the lower river in the ranges optimal for the production of salmon in the July through September period, hypoliminal water is drawn from the lake via low level intake in gradually increasing amounts to temper the epiliminial water drawn from the upper layer. (7)

Thus, the natural temperature regime of the salmon is duplicated, using density currents created by withdrawal.

An organic, bacteriological, or chemical pollutant, if it flows into a reservoir as a density current, may behave as a quasi-pipeline. It has been found that a pollutant discharged from an industrial plant flowed through Cherokee Reservoir of the TVA system as a discrete flow with a minimum of dispersal and diffusion, and the water was discharged through turbine outlets with a minimum of pollution to the reservoir storage.

The previous situations show that the management of reservoir water quality depends in large part on how well one can control the internal current regime in a reservoir.

3. Purpose and Scope of Investigation

Reservoir internal density currents have been studied by theoretical approaches, laboratory experiments, and direct measurements of velocities and stratifications on prototype reservoirs. However, the majority of these efforts have been toward the study of withdrawal currents, and little has been done with inflowing density currents. Since what flows out of a reservoir at one time was streamflow it seems that inlet streamflow effects on reservoir current regimes should merit more consideration.

In the present study, the influences of entering streamflow on the current patterns of a model stratified reservoir are reported. This study is an attempt to relate various parameters of entering streamflow at the upper end of a thermally stratified reservoir to the current regime in the reservoir for the purpose of maintaining quality control.

II. ANALYTICAL CONSIDERATIONS

Presentation of basic assumptions and equations pertaining to two-dimensional, inviscid, steady, incompressible, continuously stratified flow are given in the following section. Withdrawal currents and inflows are next discussed analytically, and finally the method of analysis used to establish the desired streamflow-current regime relationships is explained.

1. Stratified Flow Equations

Consider an incompressible fluid such as water stratified by a slight linear density gradient, as associated with the thermal structure of temperate zone reservoirs or as is created by salinity variation in an estuary. Also consider the flow of any internal currents to be two-dimensional and independent of time where x and y are the respective horizontal and vertical coordinates and u and v the velocity components in the x and y directions.

Figure 3 shows the basic stratified system. With this notation

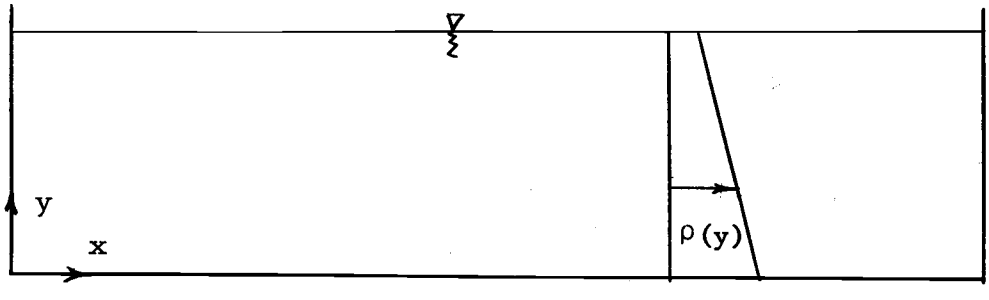

Figure 3. Basic stratified system.

the condition for incompressibility in the sense that a liquid element undergoes a negligible volume change by definition is:

$$\frac{\partial u}{\partial x} + \frac{\partial v}{\partial y} = 0. \qquad 2\text{-}1$$

The general continuity equation,

$$\nabla \cdot (\rho \overline{V}) + \frac{\partial \rho}{\partial t} = 0,$$

where

$\overline{V} = u\hat{i} + v\hat{j}$,

ρ = density,

t = time,

∇ = gradient operator,

is valid for stratification due to temperature variation, but if the stratification is due to a dissolved substance, an additional term is needed to account for mass transfer due to molecular diffusion. Molecular diffusion may be described by an observational law known as Fick's first law in which the rate of mass transfer of a substance per unit area is proportional to the gradient of concentration of the substance. Assuming Fick's first law of diffusion, the mass rate of flux per unit area is:

$$J = - \nabla \cdot [D' \nabla C]$$

where

J = mass rate of flux per unit area,

D' = diffusion coefficient,

C = concentration of substance.

The expanded continuity equation may be rewritten:

$$\frac{\partial \rho}{\partial t} + \rho(\nabla \cdot \overline{V}) + \overline{V}(\nabla \cdot \rho) = \nabla \cdot [D' \nabla C].$$

From the assumptions of steady, incompressible flow the continuity equation may be simplified:

$$u\frac{\partial \rho}{\partial x} + v\frac{\partial \rho}{\partial y} = \nabla \cdot [D' \nabla C].$$

Assume a small density variation so that the diffusion coefficient approximates a constant. Also assume a linear relationship between concentration and density so that

$$\rho - \rho_o = M(C - Co).$$

Substituting for C, the equation for the conservation of mass becomes:

$$u\frac{\partial \rho}{\partial x} + v\frac{\partial \rho}{\partial y} = \frac{D'\partial^2 \rho}{M \partial y^2} . \qquad 2\text{-}2$$

The equations of motion expressing the relationship between the inertial force per unit volume, the pressure force per unit volume, the gravitational force per unit volume, and the viscous force per unit volume are written as:

$$\text{x-direction:} \quad \rho\left(u\frac{\partial u}{\partial x} + v\frac{\partial u}{\partial y}\right) = -\frac{\partial p}{\partial x} + \frac{\partial}{\partial y}\left(\mu\frac{\partial u}{\partial y}\right); \qquad 2\text{-}3$$

$$\text{y-direction:} \quad 0 = \frac{\partial p}{\partial y} - \rho g; \qquad 2\text{-}4$$

where

p = pressure,

g = gravitational acceleration,

μ = kinematic viscosity.

From the above equations it is apparent that the driving force of internal density currents must stem from the imposition of a pressure gradient into the flow field.

Internal density currents important to a reservoir are associated with the pressure gradient formed by inflowing or outflowing discharges and should be governed by equations 2-1, 2-2, 2-3, and 2-4.

2. Withdrawal Currents

Internal density currents under conditions of withdrawal

have been studied extensively in literature, and limited analytical solutions to equations 2-3 and 2-4 under conditions of withdrawal have been attempted through work by Long(19), Yih (31), Kao (16), Koh (17), and Gelhar and Mascolo (15). Long (20) first approached the problem by assuming that the velocities involved were large enough to ignore viscous and diffusive terms. He then simplified the equations of motion to an equation for the stream function. Yih (31) showed that the equation for the stream function could be linearized by defining a transformation. The governing differential equation after transformation by Yih became

$$\frac{\partial^2\psi}{\partial x^2} + \frac{\partial^2\psi}{\partial y^2} + \frac{g\varepsilon\psi}{U^2} = -\frac{g\varepsilon}{\nu} y,$$

where

$$\varepsilon = -\frac{1}{\rho_o}\frac{\partial\rho}{\partial y} ,$$

$$\nu = \frac{\mu}{\rho} .$$

Normalizing the equation by the depth d as follows:

$$\xi = \frac{x}{d} ; \qquad \eta = \frac{y}{d} ; \qquad \theta = \frac{\psi}{Ud} ;$$

the equation transforms to:

$$\frac{\partial^2\theta}{\partial\xi^2} + \frac{\partial^2\theta}{\partial\eta^2} + \frac{g\frac{\Delta\rho}{\rho}d}{U^2}(\theta+\eta) = 0,$$

where $\frac{g\frac{\Delta\rho}{\rho}d}{U^2} = Fr^{-2}$, the inverse square of a modified Froude number. Of particular significance was that the critical values for Yih's solution occurred in terms of the modified densimetric Froude number, Fr. Yih found that for $Fr < \pi^{-1}$ this solution no longer satified upstream boundary conditions. Experiments by Debler (10) qualitatively confirmed the limits of Yih's solution and also demonstrated that where Yih's solution failed the flow patterns were in the form of definite flowing layers separated from nonflowing zones by free streamlines. Kao (16) extended the inviscid solution for $Fr < \pi^{-1}$ by altering the boundary conditions and obtained the equation for the free streamlines along with the velocity distribution. Koh (17) found a solution to the equations of motion, including both viscous and diffusive terms, by perturbation techniques. He analytically described the withdrawal layer and experimentally confirmed his results. Gelhar and Mascolo produced a solution ignoring diffusion by using the same basic assumptions as did Koh.

An example of the solution for the withdrawal layer as done by Koh (17) is shown in Figure 4.

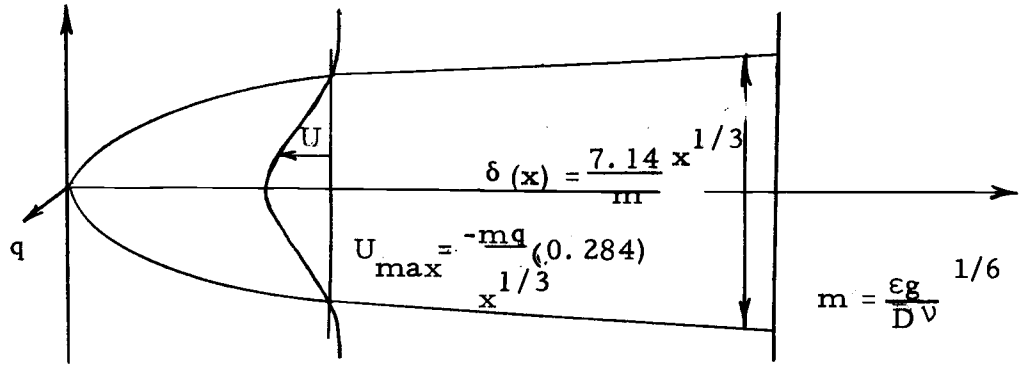

Figure 4. Withdrawal layer toward line sink. (Koh)

3. Inflow Currents

Recent literature concerning discharge into a stratified medium has been concerned with describing inflow parameters and little effort has been made to relate the effect of inflow on the current regime within the stratified medium. However, to analyze the inflow-current regime relationship it is necessary to review basic assumptions concerning the inflow. Literature pertinent to this study concerns the two dimensional turbulent or laminar jet.

Turbulent jet behavior generated by a continuous source of momentum is a fundamental case of free turbulent flows. Development of free turbulent flow in a homogeneous media is discussed extensively inSchlichting (27) , Daily and Harleman (8) and Abraham (1) . The basic assumptions in most of these treatments consider the conservation of momentum and the

assumption of Gaussian velocity and concentration distributions. Extension of free turbulent flow behavior to a stratified ambient fluid has been done by Ellison and Turner (11), Fietz (13), Wada (30), Morton (22), and Fan (12). Ellison and Turner (11) and Fietz (13) studied two-dimensional wall plumes and three-dimensional density currents, respectively, applying largely dimensional analysis techniques. Wada (30) has advanced numerical techniques for the study of cooling water flow patterns from diffusers. Most of the analytical studies of turbulent jets in a stratified fluid have resulted from an integral technique used by Morton, Taylor and Turner (23) in analyzing a simple plume in a linearly density stratified environment. Fan (12) used the Morton type analysis to obtain theoretical solutions for an inclined round buoyant jet in a density-stratified environment.

For this study consider the fully turbulent stream flowing into the density stratified reservoir as shown in Figure 5.

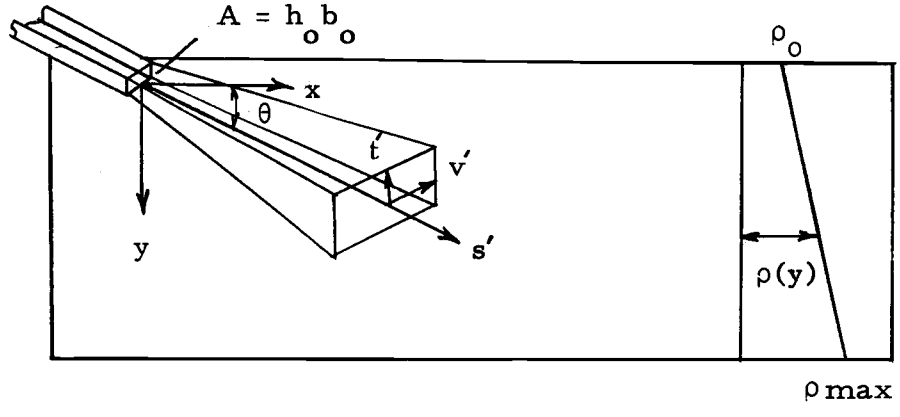

Figure 5. Rectangular jet discharging into a linear stratified medium.

An integral type analysis may be applied. The following assumptions are made:

(i) The fluids are incompressible.

(ii) The velocity distribution is a modified Gaussian distribution modified to a rectangular cross section,

$$u(s', t', v') = u(s') \, e^{\left(-t'^2/h_o^2\right)} \, e^{\left(-v'^2/b_o^2\right)} .$$

(iii) The density of the jet distribution is a modified Gaussian distribution,

$$\rho(s', t', v') = \rho(s') \, e^{\left(-t'^2/h_o^2\right)} \, e^{\left(-v'^2/b_o^2\right)} .$$

(iv) The rate of entrainment at the edge is proportional to the characteristic velocity,

$$\frac{dQ}{ds'} = (2h+2b) \, ku(s'),$$

where

k = a coefficient of entrainment.

(v) The variation in density is small in comparison with ρ_o.

(vi) Pressure is hydrostatic.

The equation of continuity, based upon the assumed entrainment assumption can be expressed as:

$$\frac{d}{ds} \int_A u(s', t', v') \, dA = \frac{dQ}{ds'} ,$$

$$\frac{d}{ds'}\int_o^\infty\int_o^\infty u(s')\, e^{\left(-t'/h_o\right)^2} e^{\left(-v'/b_o\right)^2} dv'dt' = (2h+2b)\, ku(s').$$

Integrating

$$\frac{d}{ds'}\left[u(s')\ \frac{h_o^2}{2}\ \frac{b_o^2}{2}\ e^{\left(-t'/h_o\right)^2} e^{\left(-v'/b_o\right)^2}\right]\Bigg|_o^\infty\Bigg|_o^\infty = (2h+2b)ku(s')$$

$$-\frac{d}{ds'}\left(u(s')\ \frac{h_o^2\ b_o^2}{4}\right) = (2h+2b)\ ku(s'). \qquad 2\text{-}5$$

Since the pressure is assumed to be hydrostatic and there is no other force acting in the horizontal direction, the x momentum flux should be conserved,

$$\frac{d}{ds'}\int_o^\infty\int_o^\infty \rho(s', t', v')\, u^2(s', t'. v')\cos\theta\, dv'dt' = 0$$

Substituting

$$\frac{d}{ds'}\int_o^\infty\int_o^\infty \rho(s')\ u^2(s')\, e^{-3t'^2/h_o^2} e^{-3v'^2/b_o^2} \cos\theta dv'dt' = 0,$$

Integrating

$$\frac{d}{ds'}\left[\rho(s')\ u^2(s')\ \frac{h_o^2\ b_o^2}{9}\ e^{-3t'^2/h_o^2} e^{-3v'^2/b_o^2} \cos\theta\right]\Bigg|_o^\infty\Bigg|_o^\infty = 0.$$

and assuming a small variation in density the following expression is obtained:

$$\text{x-momentum:}\quad \frac{d}{ds'}\left[\frac{\rho_o\, u^2(s')\cos\theta\, h_o^2\, b_o^2}{9}\right] = 0. \qquad 2\text{-}6$$

In the vertical direction there is a gravity force acting on the jet equal to the change of momentum flux,

$$\frac{d}{ds'} \int_o^\infty \int_o^\infty \rho(s', t', v')\, u^2\,(s', t', v')\, \sin\theta\, dv'dt'$$

$$= g \int_o^\infty \int_o^\infty \left[\rho(s', t', v') - \rho_a\,(s', t', v')\right] dv'dt'.$$

Substituting and simplifying

y-momentum:
$$\frac{d}{ds'}\left[u^2\,(s')\, \sin\theta\, \frac{h_o^2\, b_o^2}{9}\right]$$

$$= g\, h_o^2\, b_o^2 \left[\frac{\rho(s') - \rho_a(s')}{\rho_0\,(s')}\right]. \qquad 2\text{-}7$$

From geometry

$$\frac{dx}{ds'} = \cos\theta; \qquad \frac{dy}{ds'} = \sin\theta. \qquad 2\text{-}8 \text{ and } 2\text{-}9$$

The change in amount of dissolved substance in the jet must be conserved with respect to a chosen reference level due to the stability of the density gradient,

$$\frac{d}{ds'} \int_o^\infty \int_o^\infty u(s', t', v') \left[\rho_{in} - \rho\,(s', t', v')\right] dv'dt'$$

$$= (2b + 2h)\, k\, u(s') \left[\rho_{in} - \rho_a\,(s')\right].$$

Adding and subtracting $\rho_a(s')\, u(s', t', v')$ to the left side and integrating

$$\frac{d}{ds'}\left[(\rho_{in} - \rho_a(s'))\, u\frac{(h_o b_o)^2}{4} + u\frac{(h_o b_o)^2}{9}(\rho_a(s') - \rho(s'))\right]$$

$$= \left[\rho_{in} - \rho_a(s')\right]\frac{d}{ds'}\left(\frac{u h_o^2 b_o^2}{4}\right) - \frac{u h_o^2 b_o^2}{4}\frac{d\rho a(s')}{ds}$$

$$+ \frac{d}{ds'}\left[\frac{u h_o^2 b_o^2}{9}(\rho_a(s') - \rho(s'))\right] .$$

Previously from continuity

$$\frac{d}{ds'}\left[u(s')\frac{h_o^2 b_o^2}{4}\right] = 2(h(s') + b(s'))\, k\, u(s').$$

Substituting,

$$\left[\rho_{in} - \rho_a(s')\right] 2 k u(s')(h(s') + b(s')) - u\frac{(s')h_o^2 b_o^2}{4}\frac{d\rho a(s')}{ds'}$$

$$+ \frac{d}{ds'}\left[u(s')\frac{h_o^2 b_o^2}{9}(\rho_a(s') - \rho(s'))\right]$$

$$= \left[\rho_{in} - \rho(s')\right] 2 k u(s')(h(s') + b(s')),$$

the above becomes:

$$\frac{d}{ds'}\left[\frac{u(s')h_o^2 b_o^2}{9}(\rho_a(s') - \rho(s'))\right] = \frac{u(s')h_o^2 b_o^2}{4}\frac{d\rho a(s')}{ds'} . \qquad 2\text{-}10$$

With the relationship

$$b_o = mh_o \qquad 2\text{-}11$$

the problem has seven unknowns, namely,

$$u(s'),\ ho,\ bo,\ \theta,\ x,\ y,\ \text{and}\ \rho_a(s') - \rho(s')$$

and seven equations 2-5, 2-6, 2-7, 2-8, 2-9, 2-10, and 2-11. Initial conditions are:

$$u(o) = U_o;\ h(o) = h_o;\ b(o) = b_o;\ \rho(o) = \rho_{in};$$

$$\theta(o) = \theta;\ y = o \text{ and } x = o \text{ at } s=o,$$

but the solution of the system is not obtainable in closed form without the use of numerical techniques and is not presented here.

Very little literature is found (1969) concerning laminar jet flow into a linearly stratified medium, but here too, an approximate analysis may be performed on the inflow by making a few basic assumptions. Consider the case of a density flow proceeding down an incline as shown in Figure 6.

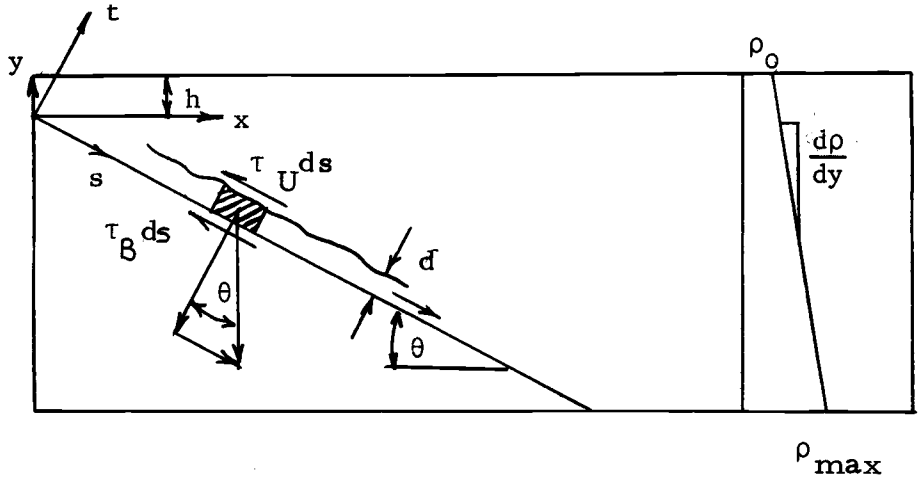

Figure 6. Density flow down an incline.

Assuming in laminar flow that the inertia terms are negligible and that the pressure gradient may be eliminated by cross differentiation, the equation of motion will contain only gravity forces and viscous forces. Summing the forces in the s-direction for the fluid element,

$$W \sin\theta = (\tau_U + \tau_B)\, ds,$$

where

τ_U = surface shear resistance,

τ_B = incline shear resistance,

$$W = \left[\gamma in - \gamma_{amb}(s)\right] d\, ds \sin\theta,$$

$$\gamma_{amb(s)} = g\left[\rho o + (h + s\sin\theta)\frac{d\rho}{dy}\right] .$$

and the shear resistance is assumed to approximate the shear relation for pipe flow.

$$\tau = \frac{\gamma in\, f\, V^2(s)}{2g} .$$

Substituting into the force summation,

$$g\left[\rho in - (\rho o + (h + s\sin\theta)\frac{d\rho}{dy})\right] d \sin\theta\, ds$$

$$= \rho in \frac{(f_U + f_B) V^2(s)\, ds}{2},$$

$$V(s) = \left[\frac{2g\, ds\sin\theta}{\rho in\,(f_U + f_B)}\left[\rho in - (\rho o + (h+\sin\theta)\frac{d\rho}{dy})\right]\right]^{1/2}$$

a relationship is obtained for V(s). Its use, however, is questioned due to the difficulty of evaluating friction coefficients, f_U and f_B. The point at which the density flow leaves the slope is obtained by the criteria that V(s) = 0,

$$V(s) = 0 \quad \text{when} \quad \rho in - \left(\rho o + (h + s\sin\theta) \frac{d\rho}{dy} \right) = 0,$$

or referenced from the water surface elevation where

$$\text{depth} = h + s\sin\theta ,$$

$$h_{curr} = (\rho in - \rho o) \frac{dy}{d\rho} .$$

This expression shows that the inflow will seek an elevation corresponding to its own density, and agrees with results that Spurkland (28) obtained with a submerged diffuser.

4. Present Study

It was reported in Section 2 that from the governing equations an analytical description of internal density currents due to the imposition of a simple pressure variation may be made. In Section 3 it was shown that in some cases an inflowing

jet may be discussed analytically if the appropriate assumptions are made. However, complete solutions are untenable when the relationship between both the inflow and the internal current regime are desired. The interaction among density, velocity, and pressure fields of the inflow and ambient fluid cause the general solution to become very mathematically complex. For this reason the density stratified reservoir flow phenomena are to be analyzed experimentally using a dimensional analysis to find correlation among the physical variables involved in this study.

Consider a streamflow entering a stratified medium with an equivalent outflow rate to maintain a constant water surface level as illustrated in Figure 7a. The independent parameters involved are those describing

(i) Boundary conditions:

D = total depth of reservoir

ϕ = angle of inflow

θ = angle of reservoir slope

h_{in} = depth of slope change

h_{out} = depth of outlet

L = length of reservoir

(ii) Inflow:

Q_{in} = inflow rate

V_{in} = inflow velocity

ρ_{in} = inflow density

b_{in} = inflow width

d_{in} = inflow depth

(iii) Outflow:

Q_o = outflow rate

V_o = outflow current velocity

ρ_{out} = outflow density

d_o = outflow diameter

(iv) Ambient fluid:

$\frac{\Delta\rho}{\Delta y}$ = density gradient

ρ_o = surface density

ρ_{max} = bottom density

(v) Miscellaneous:

g = gravitational acceleration

ν = kinematic viscosity

t = time

The dependent factors involved are those parameters describing the resulting current regime. They are:

h_1, h_2, h_3, ... the heights of various currents

v_1, v_2, v_3, ... the velocities of various currents

The densities of various currents are not included because they are related directly to the current heights.

It is known that a particular density current will be a function of the independent variables involved:

$$V_{curr} = f\left(D, S_v, S_r, h_{in}, h_{out}, L, Q_{in}, Q_o, \rho_{in}, d_{in}, \rho_o, d_o, \frac{\Delta\rho}{\Delta y}, \rho_{max}, \nu\right)$$

$$h_{curr} = f\left(D, S_v, S_r, h_{in}, h_{out}, L, Q_{in}, Q_o, \rho_{in}, d_{in}, \rho_o, d_o, \frac{\Delta\rho}{\Delta y}, \rho_{max}, \nu\right)$$

and the complexity of establishing a particular relationship is apparent from the number of parameters involved. In order to simplify the analysis a number of the independent variables as shown in Figure 7b will be held constant. Once the flow

configuration becomes known, the number of parameters involved will be further reduced in number by individually considering each main internal current allowing nonpertinent parameters to be disregarded. The functional relationships will be established in chapter IV.

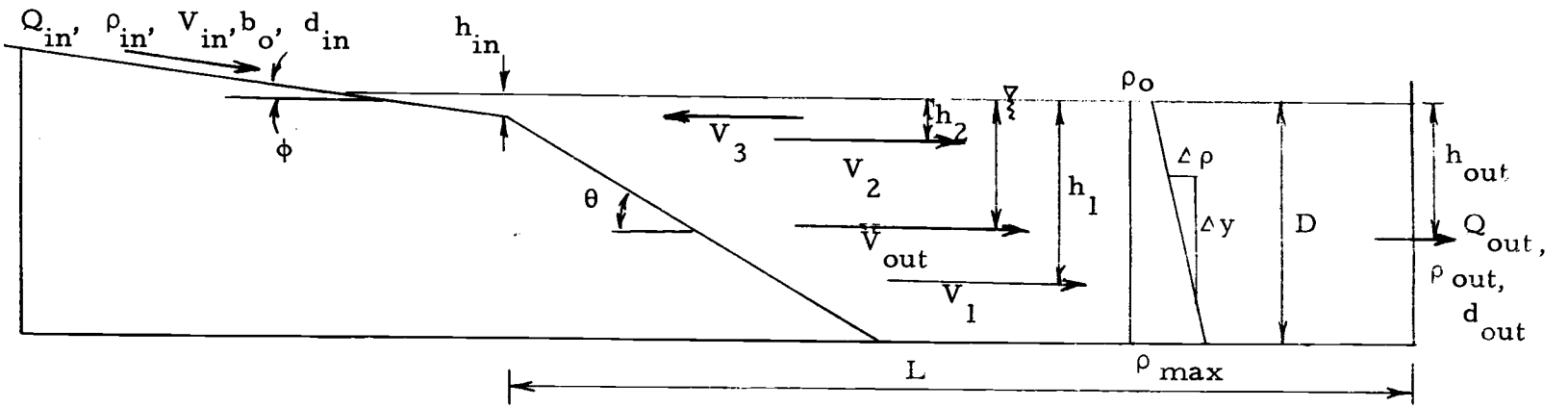

Figure 7a. Parameters involved in the investigation.

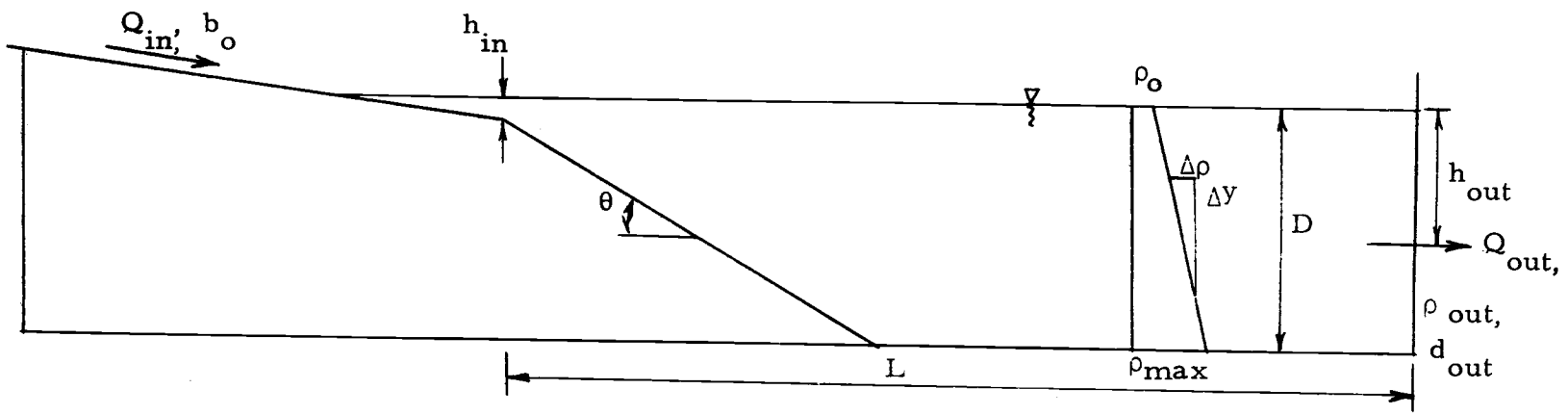

Figure 7b. Independent parameters held constant during the investigation.

III. APPARATUS AND PROCEDURE

To investigate the influence of entering streamflow on the current regime of a model density stratified reservoir a series of laboratory experiments was performed in which fluid was allowed to enter a tank of stratified fluid by way of a model streambed.

In this chapter the experimental procedure and apparatus used for the experiments will be discussed. The individual steps in the experimental procedure will be explained in detail.

1. General Description of the Procedure

For the series of experimental runs, the model reservoir was first filled with distinct layers of water containing appropriate quantities of salt (NaCl) in suspension to give a linear density gradient from the top to bottom levels of the tank. The water was then allowed to stand several hours so that the density profile would become linearly smooth by molecular diffusion. The density profile was measured indirectly shortly before each run, and after each run by measuring the electrical conductivity of the solution at various levels in the reservoir. Salt solution was mixed with water in the inflow storage tank until the desired inflow conductivity was reached. Inflow and discharge rotameters were

opened and the flow rates adjusted to be equal. After waiting for the system to reach a steady state (five minutes), dye (Erioglaucine A Supra) was injected into the inflow fluid in order to trace its movements through the model. To observe the current patterns within the model, dye particles were intermittently dropped into the model reservoir at a reference station. As the dye particles fell, they left a distinct vertical time line. Thirty-five millimeter slides taken at various time intervals and a time lapse movie camera recorded the horizontal motions of the time lines. Typical exposures are shown in Figure 8. An overhead movie camera photographed at various time intervals the entering inflow configuration and its travel. Each run lasted two hours at which time the tank was drained, washed, and set up for the next run. The necessary velocity and configuration measurements were obtained from the film record.

2. The Model Reservoir and Model Stream.

The reservoir for the inflow experiments was a clear walled, rectangular, plexiglas flume. It was 25 feet long, 18 inches wide, and 22 inches deep. A schematic drawing and a photograph of the reservoir are shown in Figures 9 and 10, respectively. The inlet end was equipped with an adjustable bottom slope so that the depth varied from zero to full depth at different possible choices of slope.

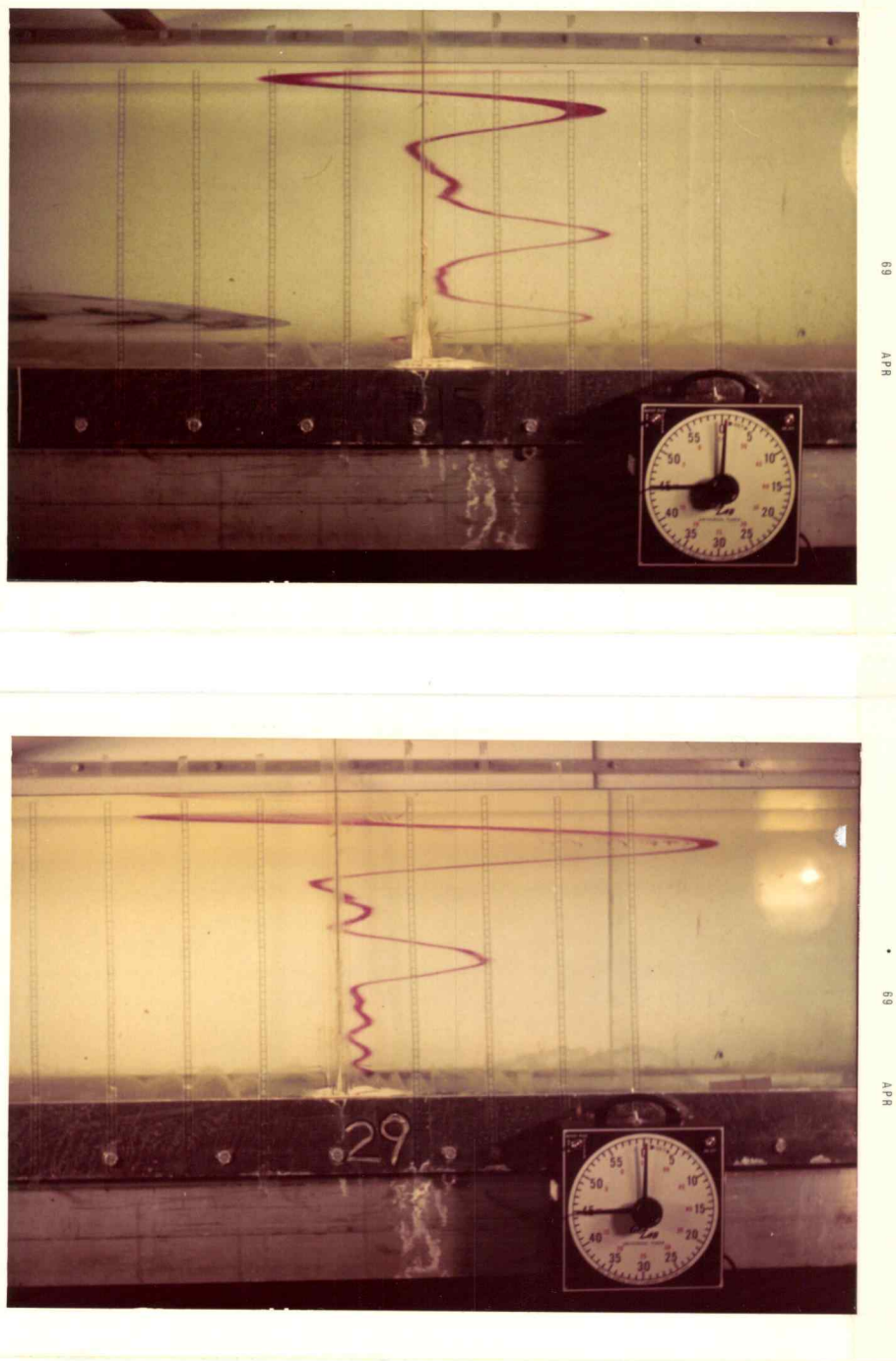

Figure 8. Typical photographs of time lines

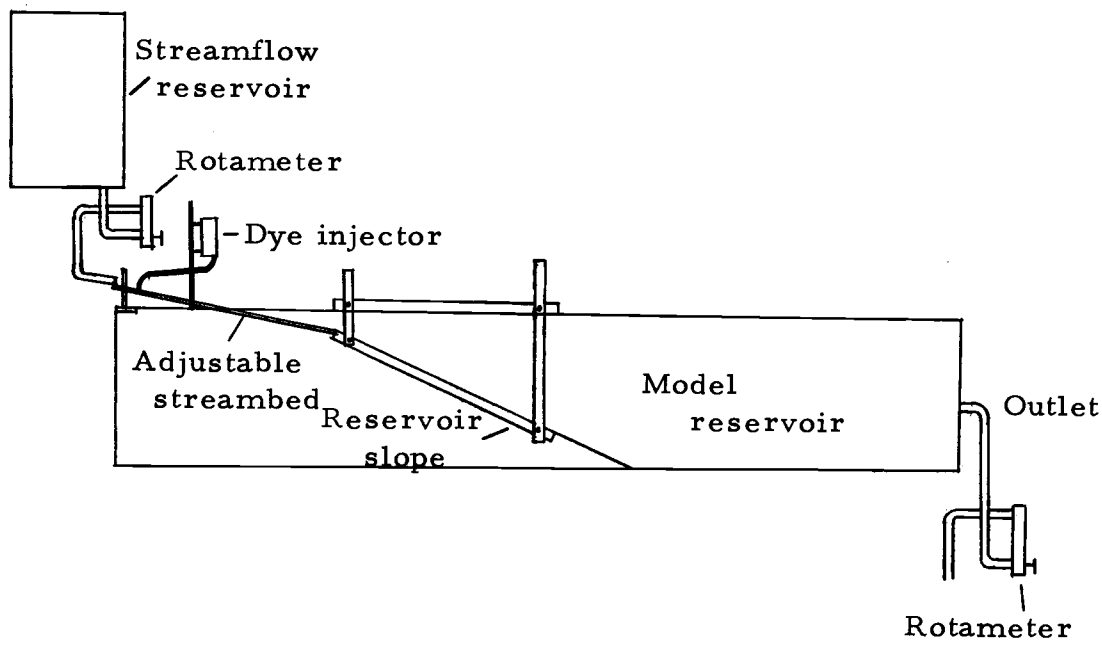

Figure 9. Schematic plan of model reservoir and streambed.

The simulated stream channel was a six foot length of 2"x1"x1/8" aluminum channel mounted on a sheet of plexigas which fit snugly in the width of the tank. The aluminum channel and plexiglas sheet was used as a second slope extending from the end of the tank to the top of the bottom slope. The configuration of two slopes was necessary to provide a continuous slope from above the water surface to the bottom of the tank while maintaining a flat slope for the simulated streambed. The flow for the simulated stream was provided by a storage tank at the upper end of the model reservoir. The water from this tank was released at the upper end of the model stream. The stream was lined with cemented sand grains to provide artificial roughness.

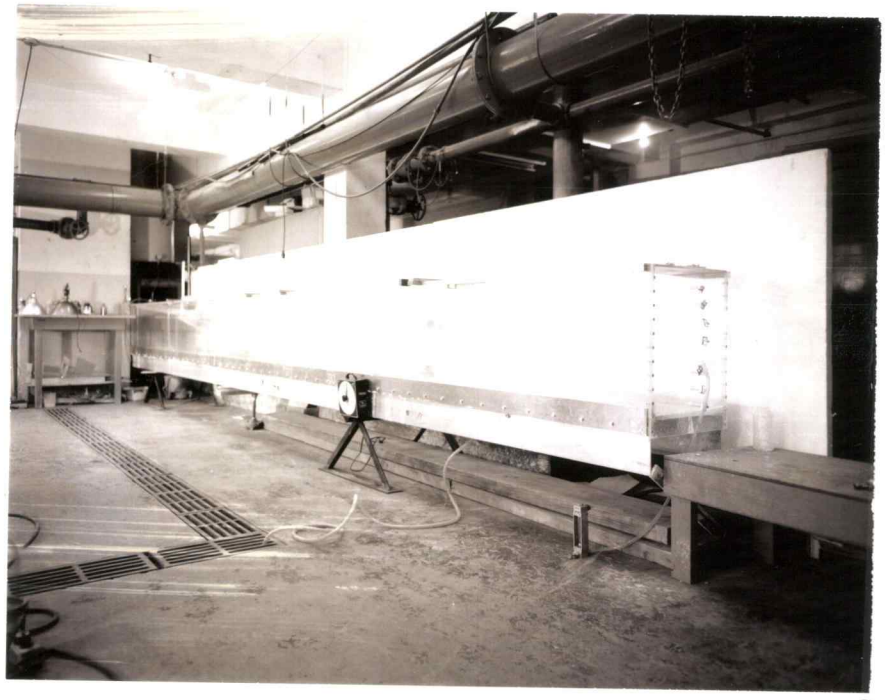

Figure 10. Photograph of model reservoir and streambed

3. The Filling Apparatus and Procedure

The desired linear density profile was achieved by mixing measured amounts of a saturated salt solution with a fixed amount of water in a mixing tank, and placing the mixture in the reservoir. The basic apparatus by Spurkland (1968) was redesigned and used for this purpose.

A typical filling cycle began with the activation of a timing cam system by a Lapine multispan timer which was set to provide power for the duration of the filling cycle. Each mixing cycle lasted 40 minutes and involved the opening and closing of the salt tank, water supply, and mixing tank solenoids. The amount of salt brine for each ten mixing cycles was controlled by ten 20-minute sequential timing cams, each activated by a 40 minute cycle timing cam and a pressure switch that shut the water off when the water surface reached a certain level. The draining of the mixing tank was accomplished by another 40 minute cycle timing cam calibrated to the draining time of the mixing tank. A block diagram of the automatic filling apparatus is shown in Figure 11. The salt solutions were introduced into the model reservoir by gravity flow through three stand pipes placed on the floor of the tank. The model reservoir was set on a very mild slope. As additional inflowing layers are

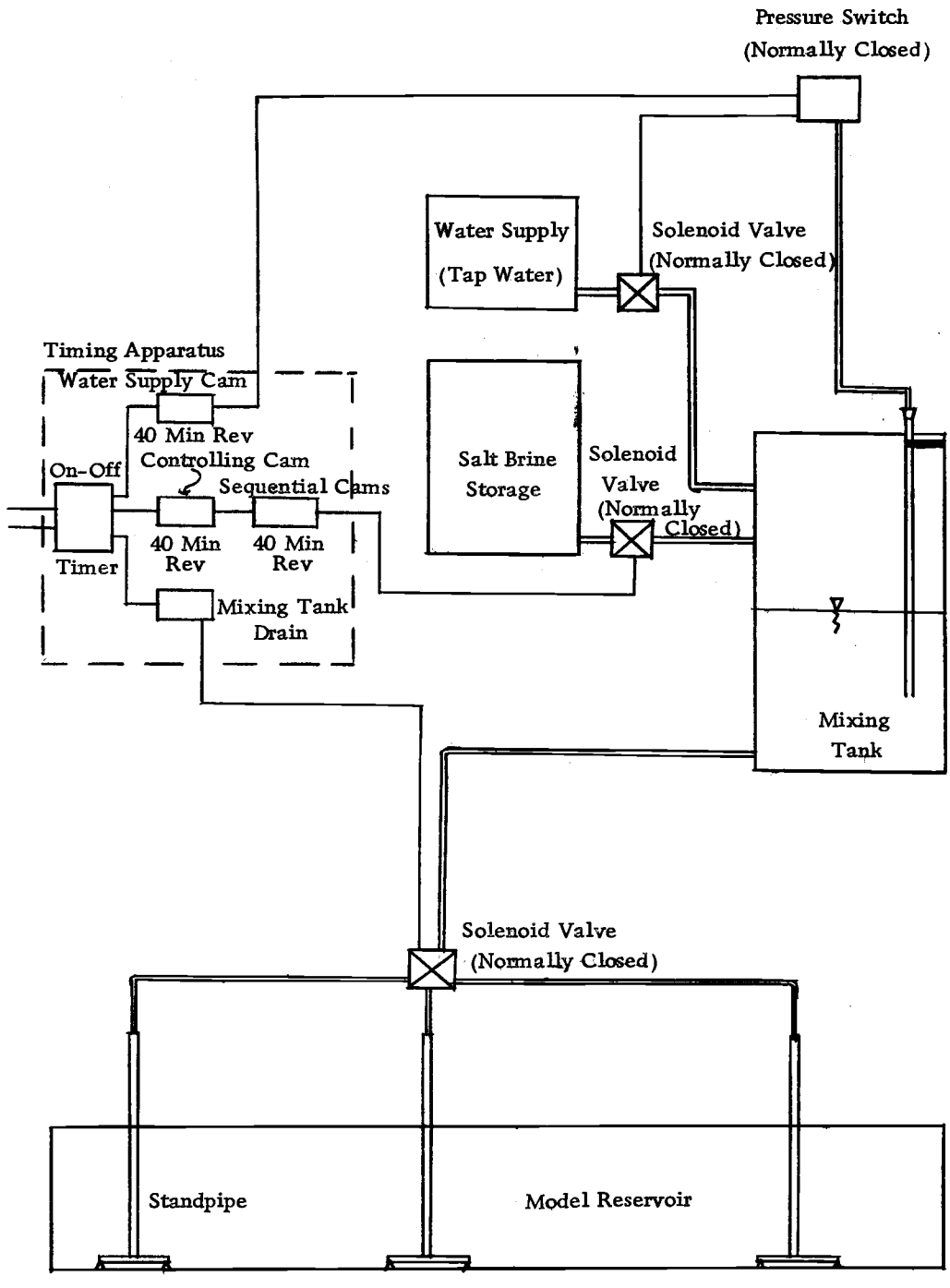

Figure 11. Schematic of filling apparatus

progressively more dense, they flow slowly by gravity along the bottom of the channel under the other layers creating a minimum amount of mixing.

4. Photography

Because of the complexity of the events during each two hour run, photography was used to record much of the data. An Argus C-3 35mm camera and a Nizo S-80 super 8mm camera were used to photograph the vertical dye streaks, and another Nizo S-80 super 8 mm camera was mounted overhead to observe the inflow configuration. All cameras were used with Kodachrome II color film at ASA 40 in conjunction with photoflood lights. The 35 mm camera had a 50mm Argus Cintar f3.5 lens while the 8mm cameras had a 10mm-80mm zoom f2.8 lens which was used at 10 mm.

The tank had a 12:1 length to depth ratio, so the cameras field of view covered a limited area. A reference station was established 10.5 feet from the mouth of the model stream, and the horizontal cameras were positioned in respect to it. A clock mounted near the wall of the model reservoir gave elapsed time as recorded on film. An overhead camera was positioned over the model stream mouth. A schematic drawing of the positioning and coverage is shown in Figure 12.

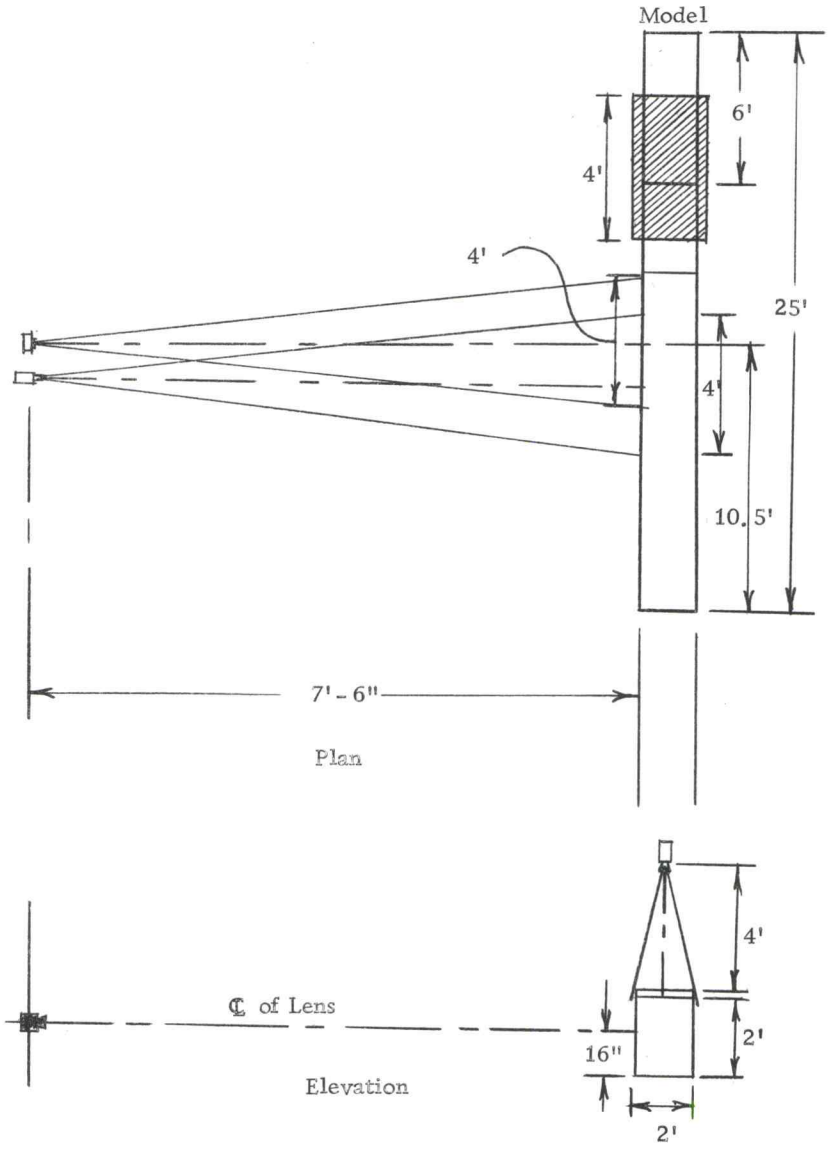

Not Drawn to Scale

Figure 12. Positioning of cameras and respective fields of view

5. Measurement of Density Profiles.

A conductivity probe and a Serfass Conductivity Bridge was used to measure the electrical conductivity of the salt solution as a measure of its density prior to and after every run. Several investigators have used the exposed conductivity probe in conjunction with a conductivity bridge with much success as seen from Spurkland (28) Lofquist (18) , and Rumer (26) . From their conclusions it is desirable to use a small platinized probe so that polarization and capacitance effects would be minimized. The probe used in this study was made of two $1cm^2$ platinum plates, spaced one cm apart as shown schematically in Figure 13. The probe was connected to the conductivity bridge by leads running through a water-tight glass tube indexed in a

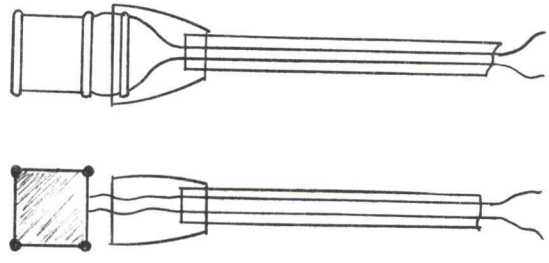

Figure 13. Conductivity probe.

centimeter scale. The conductivity was measured vertically at two centimeter intervals in the centerline of the tank. To obtain conductivity-density relationship the probe was periodically calibrated with a Christian Becker balance reading specific gravity directly. A typical density profile and the corresponding calibration curve are shown in Figure 14.

6. Measurement of Flow Rates

After the conductivity profile had been measured, a Brooks rotameter was adjusted at both the inflow and discharge ends of the model reservoir to maintain a constant inflow and outflow rate of 12.6 cubic centimeters per second. Since the rotameters were originally calibrated for a specific gravity of 1.000, they were re-calibrated for each of the five specific gravity values used in this study. The calibration is shown in Figure 15. Although this plot indicates a small density influence on the flow rate, it is small enough relative to the error inherent in reading the rotameter that it may be ignored.

7. Measurement of Velocities

After the flow attained a quasi-steady state (five minutes), potassium permanganate crystals mixed with carbon tetrachloride were dropped into the model reservoir at the reference station

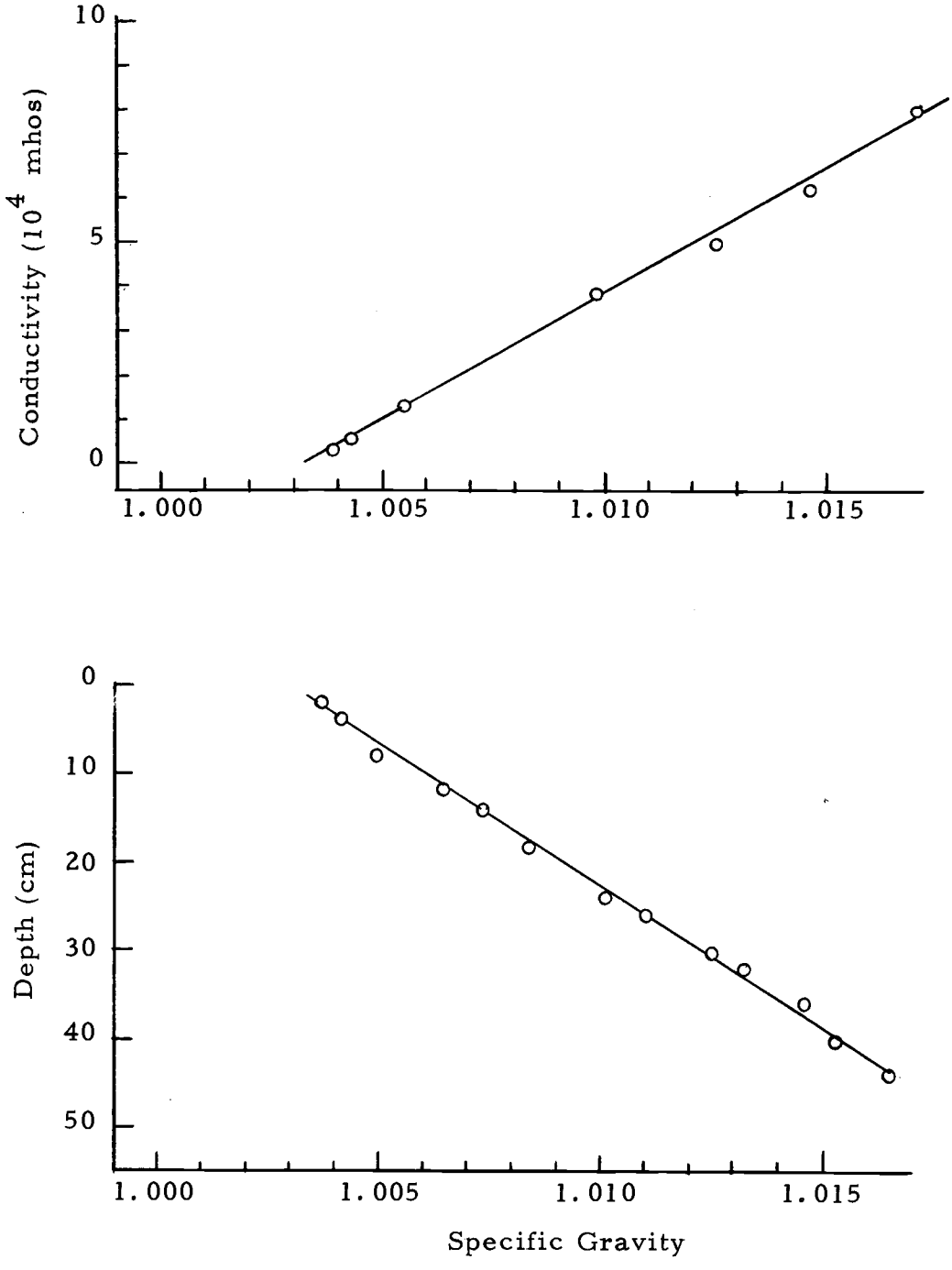

Figure 14. Calibration curve and density profile for run number 21.

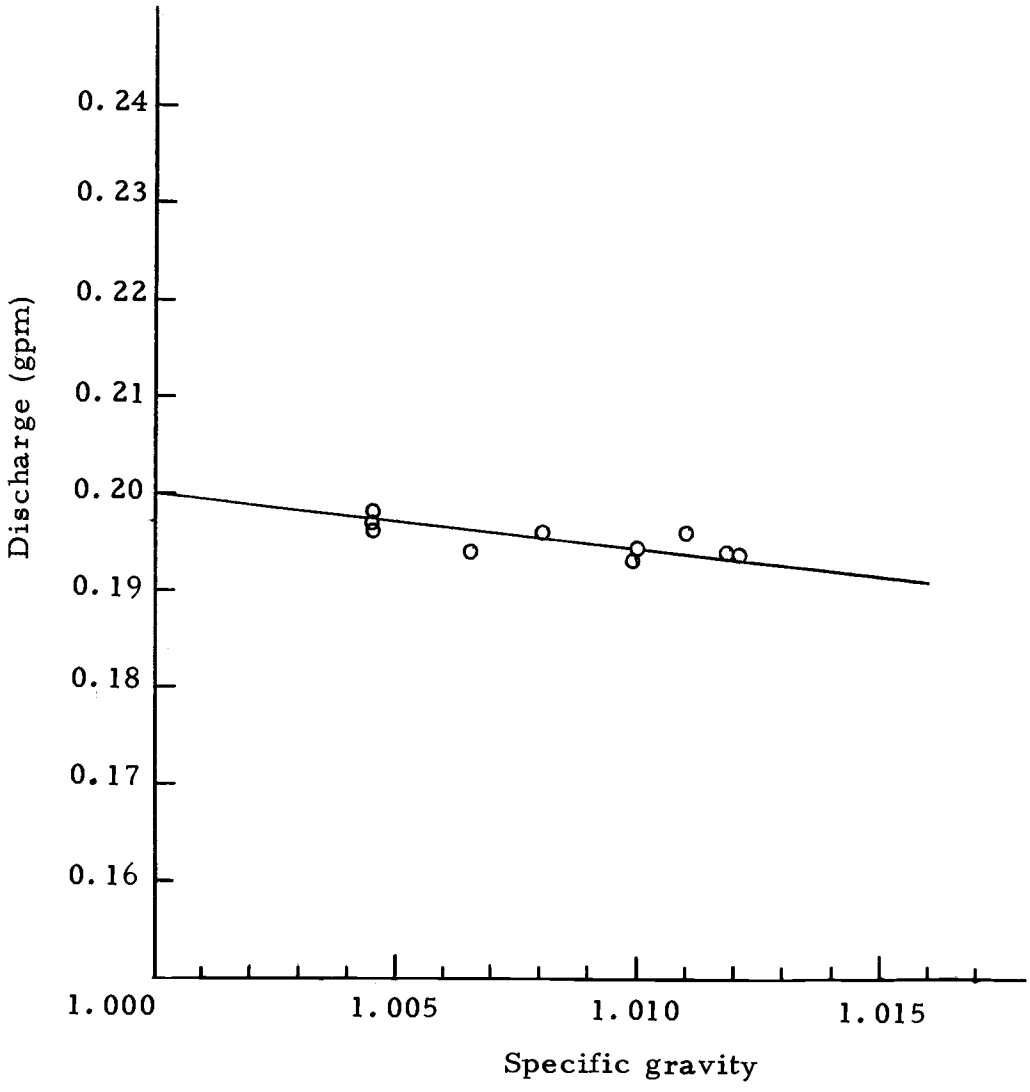

Figure 15. Calibration of inflow rotameter.

forming time lines which deform with the currents. A new time line is injected every 20 minutes for the two hour period. At least 20 slides were taken at regular time intervals and the movie camera was run continually at one frame every two seconds. After the film was developed the frames were projected into a viewing box constructed as shown in Figure 16. Time of travel measurements were taken from a grid after establishing the scale of the image projecting the picture distance between the flume's bolts at a constant scale. Measurements were taken near the center of the projected area to minimize parallax.

The overhead camera was operated at 18 frames per second during four intervals in the two hour run. Time of travel measurements of the inflow stream velocity and the inflow density current were obtained by projection and frame counts.

Figure 16. Projection apparatus for viewing time lines

IV. EXPERIMENTAL RESULTS

Twenty experimental runs were performed with the previously described apparatus to determine the relationship between the entering streamflow and the model reservoir current patterns. The resulting current regime produced in the model reservoir is described, and correlations are established between the observed current parameters and the inflow characteristics for each of the main currents.

1. General Current Patterns

As the entering streamflow, designed Q_{in}, flowed down the sloping streambed and entered the initially static, density-stratified, model reservoir, certain major repetitive current patterns were created. At the lowest streamflow velocities, V_{in}, little mixing occurred between the ambient fluid and the streamflow, and the majority of the streamflow density current proceeded down the reservoir slope until reaching a reservoir depth having equivalent density. At this point the streamflow density current flowed horizontally across the reservoir and became the main inflow current, Q_1. At the higher streamflow velocities more mixing occurred creating a large mixing current, Q_3; and at the highest streamflow velocities, mixing was so

extensive that very little of the entering streamflow discharged down the reservoir slope. As the mixing current, Q_3, increased, a reverse current at the surface, Q_4, caused by entrainment to the mixing current occurred, and an eddy in the vicinity of the stream mouth was consistently formed. A fourth current, Q_2, was formed by the outflow necessary to keep the water surface elevation constant. A typical or general current pattern existing in the model reservoir during a test run is indicated in Figure 17.

Occasionally small intermediate currents were noticeable between the major currents shown in Figure 17, but these were relatively minor in magnitude and did not consistently appear so they were not analyzed further.

The reverse current, Q_4, was not analyzed either because of the difficulty in observing the point of maximum velocity of the dye trace which coincided with the water surface.

2. The Main Inflow Current

The major inflow current at low inflow velocities was Q_1. The pertinent independent variables involved in establishing a dimensionless correlation between the current depth, h_1, the maximum velocity, $\overline{V}_{1\,max}$, and the inflow characteristics are:

$$h_1 = f\left(\rho_{in} - \rho_o,\ V_{in},\ g,\ \nu,\ \frac{\Delta\rho}{\Delta y},\ D,\ b_{in},\ d_{in}\right)$$

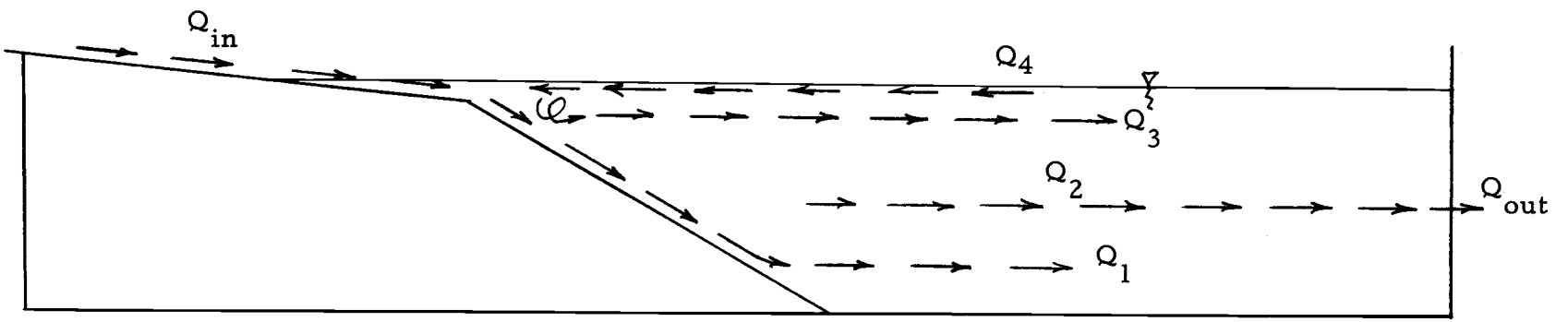

Figure 17. General current pattern

and $$\bar{V}_{1\,max} = f\,(\rho_{in} - \rho_o,\ \frac{\Delta\rho}{\Delta y},\ g,\ Q_{out},\ b_{in},$$

$$h_1,\ D,\ h_{out},\ b)$$

Using the Buckingham π theorem the dependent variables may be made dimensionless and written as a function of a number of dimensionless groupings involving the independent variables:

$$Y_1(h_1) = \phi\left(\alpha_1^{A_1}, \alpha_2^{B_1}, \alpha_3^{C_1}, \ldots \alpha_{n-r}^{X_1}\right),$$

and $$Y_2(\bar{V}_{1\,max}) = \phi\left(\beta_1^{A_2}, \beta_2^{B_1}, \beta_3^{C_2}, \ldots \beta_{n-r}^{X_2}\right),$$

but there are several dimensionless groups involving h_1, and $\bar{V}_{1\,max}$, and consequently many different possible groupings for each α and β. Also, since $\alpha_1 \ldots \alpha_{n-r}$ and $\beta_1 \ldots \beta_{n-r}$ are dimensionless, they may group with each other in any possible combination. However, from experience and consideration of the type of variables involved, functional relationships would be expected to be influenced largely by the following criteria:

$$Re = \frac{VL}{\nu},$$ a form of Reynolds number;

$$Fr = \frac{V}{(gh)^{1/2}},$$ a form of Froude number;

$$\frac{a}{b},$$ a geometric ratio;

$\frac{\rho_{max} - \rho_o}{\rho max}$, a density ratio.

The correct form of the relationship for h_1, was found to be:

$$\frac{h_1}{D} = \phi\left(\frac{V_{in} b_{in}}{\nu_{in}} , \frac{\rho_{in} - \rho_o}{D} \quad \frac{\Delta y}{\Delta \rho}\right) .$$

The dimensionless depth, $\frac{h_1}{D}$, was dependent upon $\frac{V_{in} b_{in}}{\nu_{in}}$ only in that for $\frac{V_{in} b_{in}}{\nu_{in}} > \left(\frac{V_{in} b_{in}}{\nu_{in}}\right)_{critical}$, the current, Q_1 did not exist. Figure 18 is a dimensionless plot of the depth current, Q_1, versus a density parameter for $\frac{V_{in} b_{in}}{\nu_{in}} < \left(\frac{V_{in} b_{in}}{\nu_{in}}\right)_{critical}$. The plot also shows data from Spurkland's (28) work with an under water diffuser. The difference in the relationships is due to the increased mixing associated with flow passing through the free surface which lessens the density of the inflow. The critical Reynolds number, $\left(\frac{V_{in} b_{in}}{\nu_{in}}\right)_{critical,}$ was evaluated from the relationship obtained for $\bar{V}_{1\ max}$.

The maximum velocity, $\bar{V}_{1\ max,}$ of the inflow current, Q_1, was plotted in the form of a Reynolds number against the streamflow Reynolds number in Figure 19. From this plot a relationship is seen between the two parameters, but it varies parametrically with density. Also a reinforcement of Q_1 by the

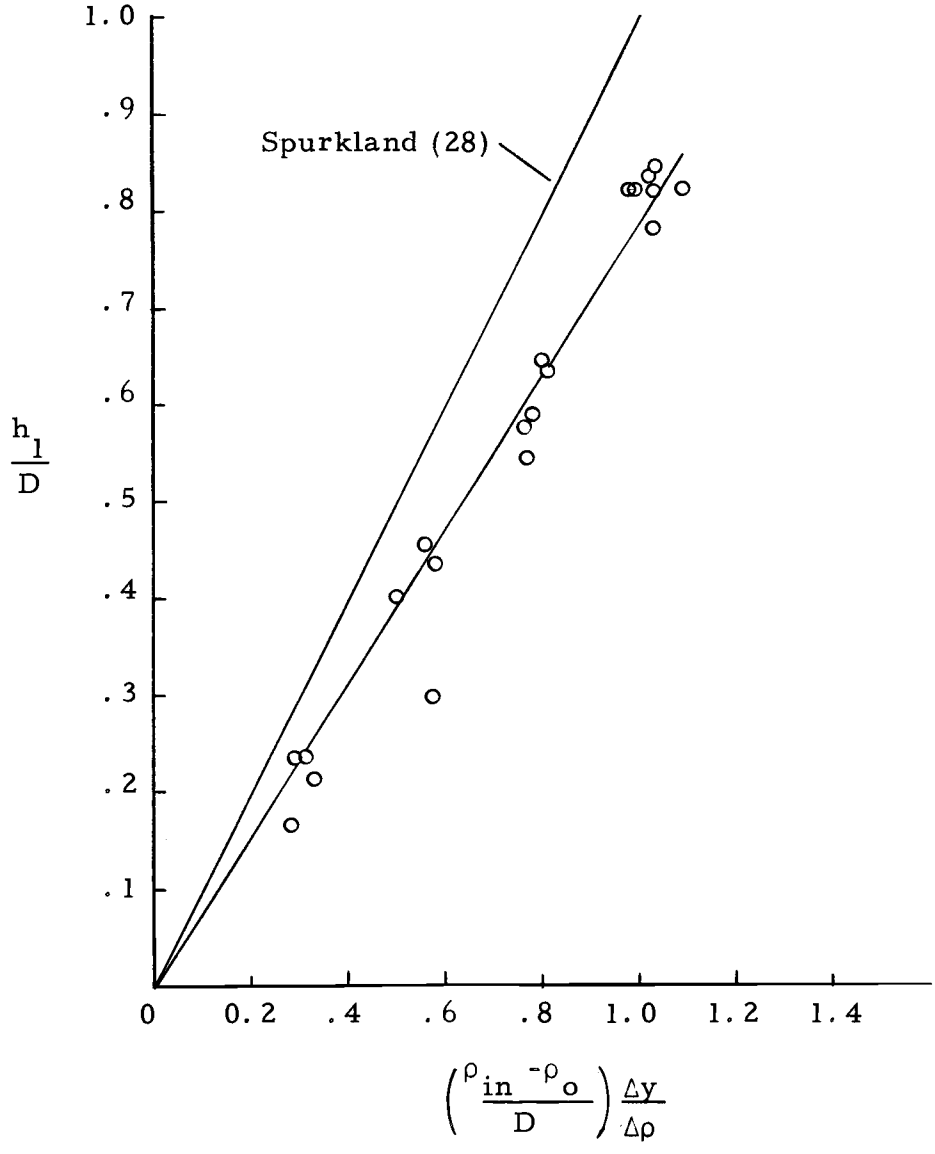

Figure 18. Depth of Q_1 versus density parameter

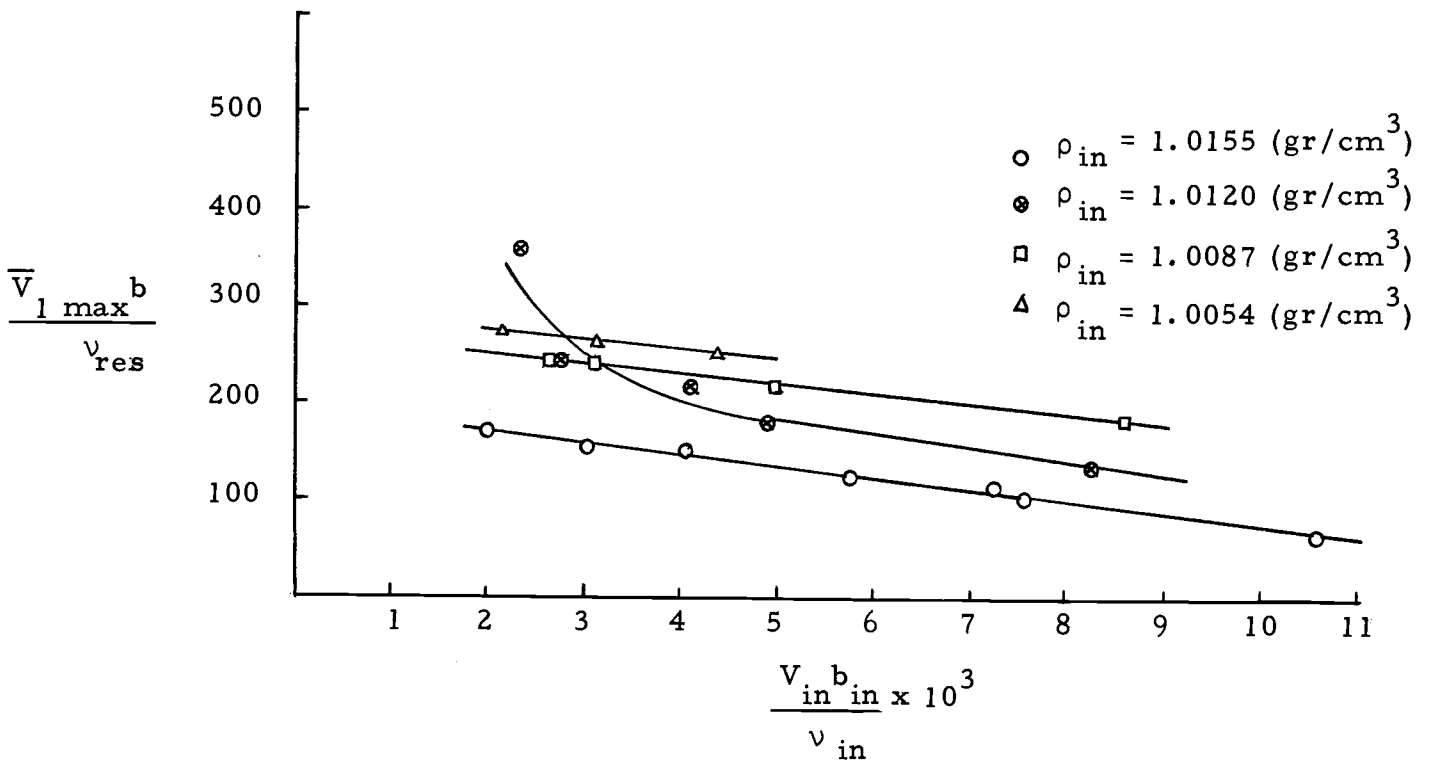

Figure 19. Streamflow Reynolds numbers versus Reynolds numbers of Q_1

withdrawal current was noticed for an inflow density $\rho_{in} \approx 1.0120$ gr/cm^3. A density scaling factor in the form of $\frac{D}{D-h_1}$ was used and the new relationship is shown in Figure 20. The plot shows that:

$$\frac{\bar{V}_{1\,max}\, b}{\nu_{res}} = \phi\left(\frac{V_{in}\, b_{in}}{\nu_{in}}\,,\ \frac{D}{D-h_1}\right) .$$

The above relationship was plotted on a semilogarithmic scale (Figure 21). The range of data obtained is nearly monotonical and fit by a straight line on this plot; although to be meaningful, $\frac{\bar{V}_{1\,max}\, b}{\nu_{res}}$ must approach a maximum value as $\frac{\bar{V}_{in}\, b_{in}}{\nu_{in}}$ approaches zero. The data did not extend into this region. The upper limit of stream-flow Reynolds number for the existence of Q_1, however, was evaluated by extrapolating the curve to $\bar{V}_{1\,max} = 0$. The relationship for $\bar{V}_{1\,max}$ for $3000 < \frac{V_{in}\, b_{in}}{\nu_{in}} < \left(\frac{V_{in}\, b_{in}}{\nu_{in}}\right)_{critical}$ and the evaluation of the critical Reynolds number are as follows:

$$\bar{V}_{1\,max} = \frac{\nu_{res}}{b}\left[-0.5\ \mathrm{Log}\left[\left(\frac{V_{in}\, b_{in}}{\nu_{in}}\right)\left(\frac{D}{D-h_1}\right)\right] + 365\right] ,$$

and $(R_e)_{critical} = \left(\frac{V_{in}\, b_{in}}{\nu}\right)_{critical} = 1.66 \times 10^5 \left(\frac{D-h_1}{D}\right)$.

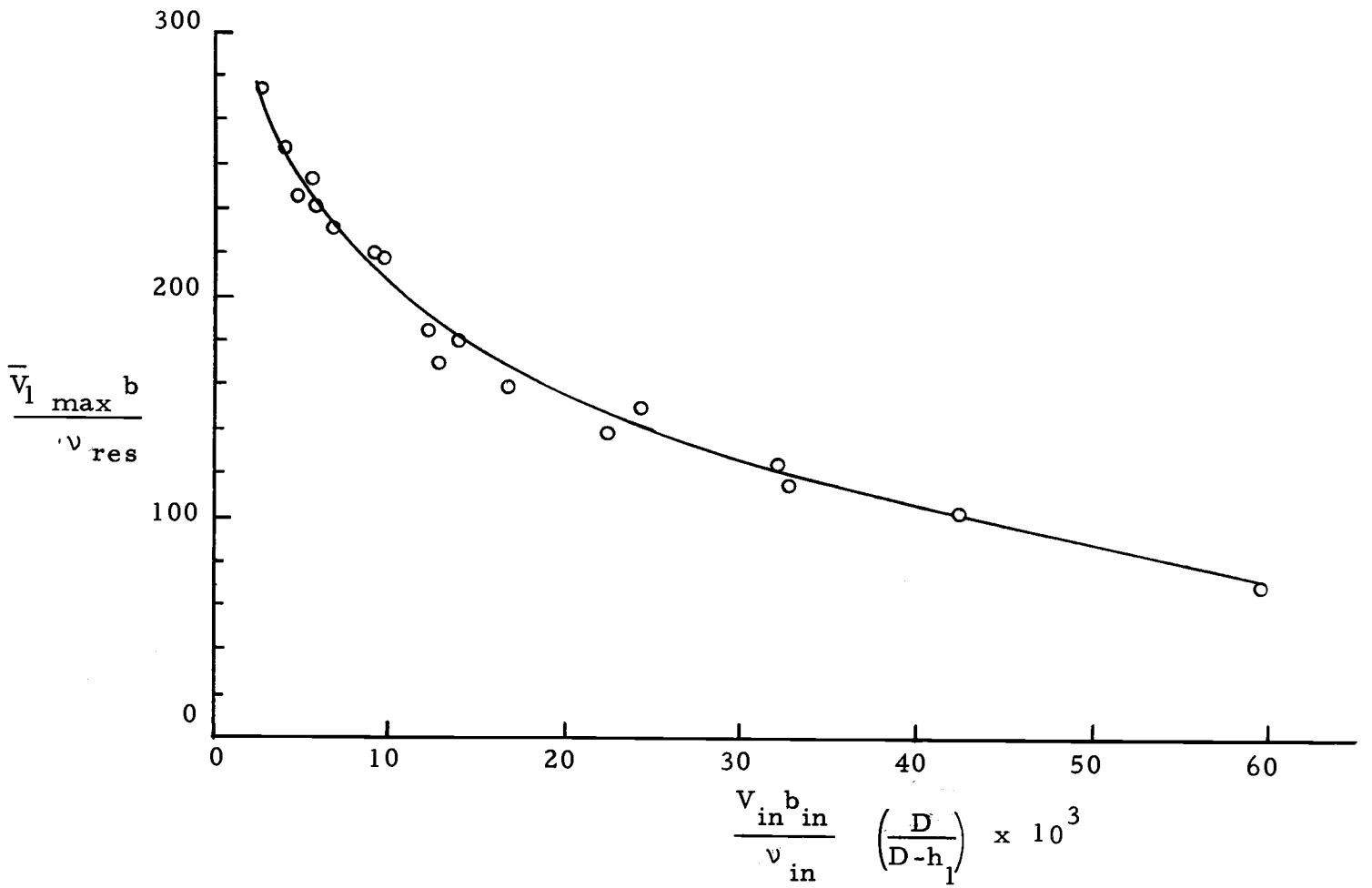

Figure 20. Modified streamflow Reynolds number versus Reynolds number of Q_l

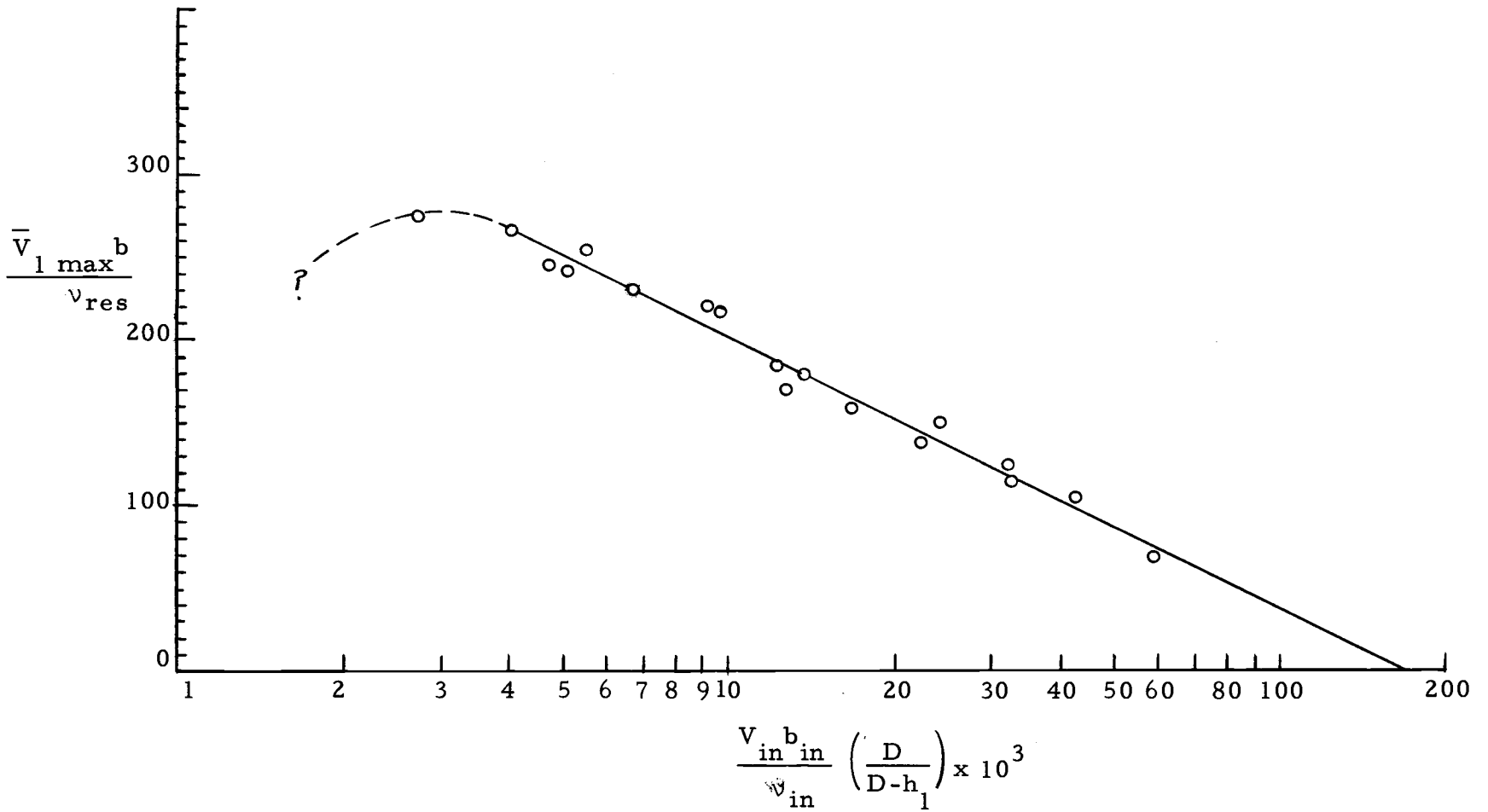

Figure 21. Logarithmic plot of scaled streamflow Reynolds number versus the Reynolds number of Q_1

3. The Mixing Current.

The major reservoir current at high streamflow velocity was the mixing current, Q_3. The pertinent independent variables involved in establishing the inflow-current relationship are similar to those in the previous section,

$$h_3 = f(h_{in}, Q_{in}, V_{in}, \rho_{in}, S, \frac{\Delta\rho}{\Delta y}, \nu_{in}, g, \rho_o),$$

and

$$\overline{V}_{3\,max} = f(Q_{in}, V_{in}, S, \frac{\Delta\rho}{\Delta y}, \nu_{in}, g, \rho_{in}, \rho_o, D, b_{in}).$$

It was expected that the depth, h_3, of Q_3 would follow a relationship of the following form:

$$\frac{h_3}{D} = \phi\left(\frac{V_{in} b_{in}}{\nu_{in}}, S, \frac{\rho_{in} - \rho_o}{D}\frac{\Delta y}{\Delta\rho}, f(Q_{in}), \frac{h_{in}}{D}\right),$$

but it is shown in Figure 22 that the depth of the mixing current, h_3/D, was independent of all varied independent variables. From this behavior, it must be concluded that h_3/D must be a function of variables held constant in this study or

$$\frac{h_3}{D} = \phi\,(Q_{in}, h_{in}).$$

No attempt was made to find this relationship.

The maximum velocity of the mixing current, Q_3, was found

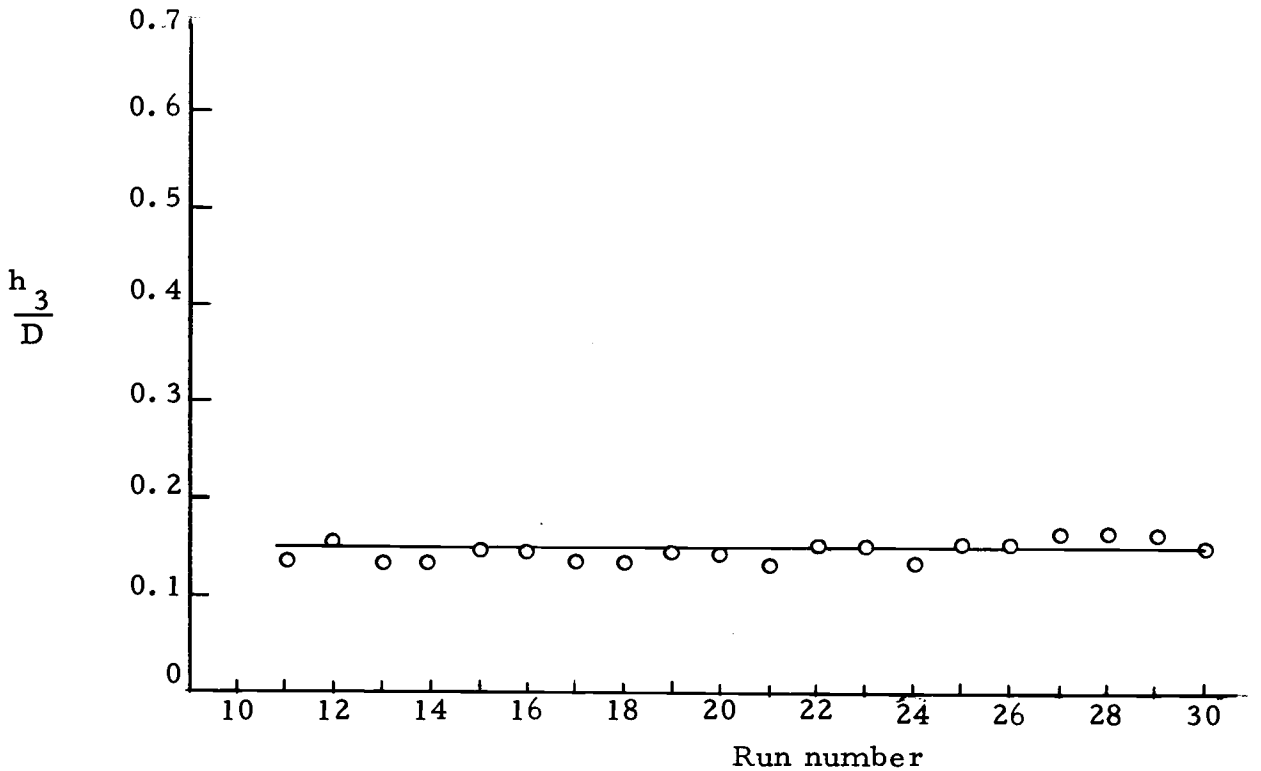

Figure 22. Depth of Q_3 versus experimental run number

to be independent of the density of the incoming fluid. Figure 23 is a dimensionless plot of the mixing current, densimetric Froude number versus the streamflow Reynolds number. The plot shows that the relationship is linear through the range of data obtained. The Froude number must approach zero as the Reynolds number approaches some value to be meaningful, but unfortunately insufficient data fell in this region to establish a criterion for the initiation of the mixing current. However, a linear relationship may be provided for a limited range of streamflow Reynolds numbers. The relationship (Figure 23) is

$$\bar{V}_{3\,max} = \left[\left(\frac{\rho_{max} - \rho_o}{\rho_{max}}\right) h_3 g\right]^{1/2}\left[1.67 \times 10^{-4} \frac{V_{in} b_{in}}{\nu_{in}} + 0.42\right],$$

$$\text{for } 2000 < \frac{V_{in} b_{in}}{\nu_{in}} < 11,000.$$

4. The Withdrawal Current

The withdrawal of water from the model reservoir, although intended to be a simplifying step by maintaining a constant water surface elevation during the duration of the experimental run, created a withdrawal current at the elevation of the outlet which extended up the length of the model reservoir. The outlet level was placed about mid-depth in the reservoir and held constant in order to distinguish the effect of the withdrawl current, Q_2, is shown in

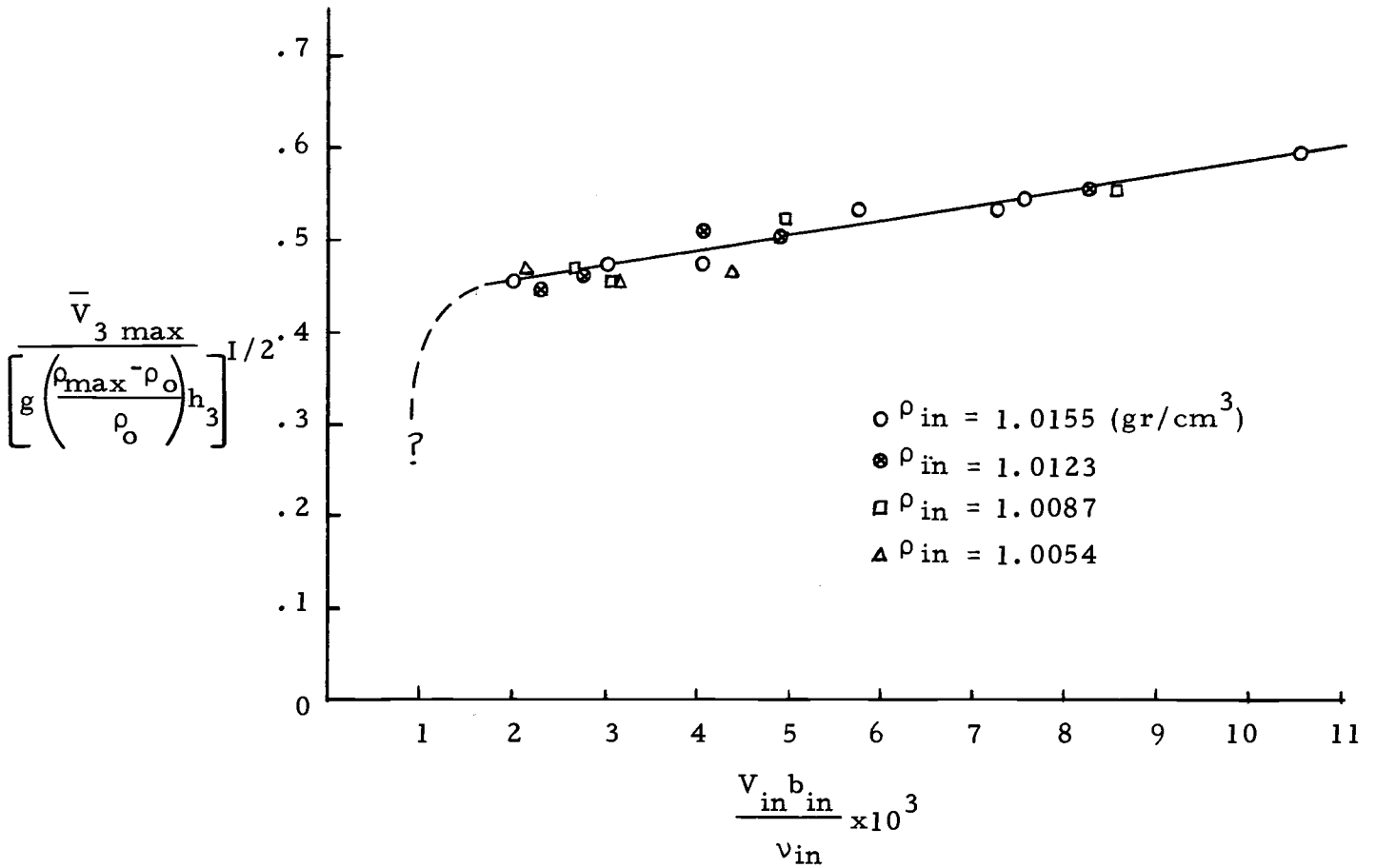

Figure 23. Densimetric Froude No. of Q_3 versus streamflow Reynolds numbers

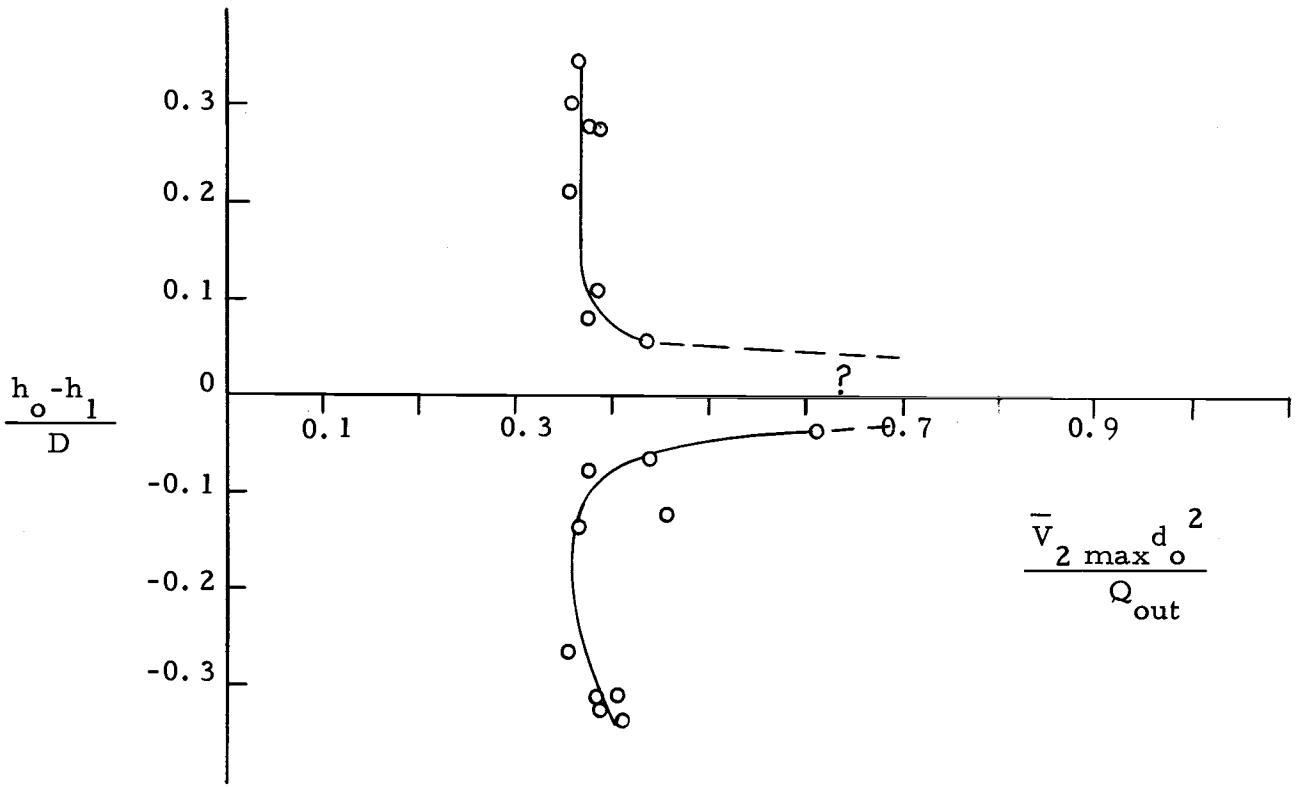

Figure 24. Difference in elevation between Q_1 and the reservoir outlet versus the velocity of Q_2

Figure 24. The figure shows a dimensionless plot of the difference in elevation of Q_1 and Q_2 versus the maximum velocity, V_2, of the withdrawal current for a constant Q_{in} and Q_{out}. The reinforcing action of the combined Q_1 and Q_2 is easily seen. No attempt was made to reproduce this plot for various Q_{in} and Q_{out}.

5. Blocking

If the flow patterns were allowed to continue longer than a two-hour period Q_1 was affected by the influence of the end of the model tank. Blocking of the current occurred and the withdrawal current began pulling out the entering streamflow as shown in Figure 25. The blocking effect was similar to that blocking described by Spurkland (28).

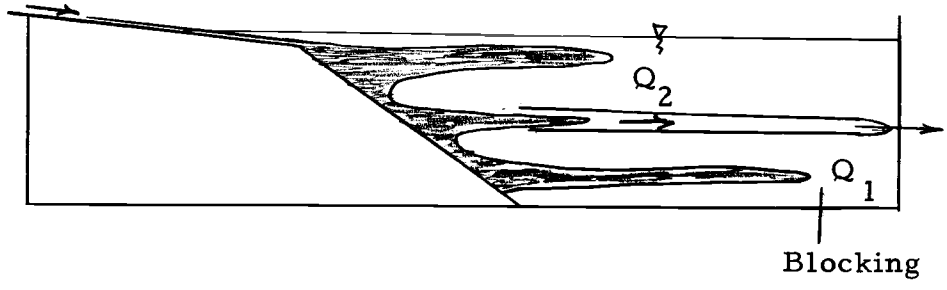

Figure 25. Influence of Q_2 on the inflow after the blocking of Q_1.

V. DISCUSSION OF THE RESULTS

Some of the effects of entering streamflow on the currents of a density stratified model reservoir were demonstrated in the previous chapter. Correlations between the entering streamflow and the resulting reservoir currents were detailed and some critical parameters established.

In this chapter discussions of errors involved in measurement of the various quantities; limitations present in the investigation; model-prototype relationships; and suggestions for further study will be presented.

1. Summary of Experimental Errors

It is generally realized that errors will be present in making any type of measurement. The probable error present in measuring flow rates, velocities, densities, viscosities, and depths in this study can be estimated as follows in Table 1. The allowable tolerances for the flow rates and length parameters were estimated from the rotameter scale and the various length scales used, while the tolerance for the average streamflow velocity was estimated from the frame speed of the movie camera.

It was first thought that variation in temperature of salt concentration might induce considerable variation in the density or

Table 1. Allowable tolerances in experimental measurements.

Tolerance	Units	Magnitude of average measurement
$Q_{in} \pm 0.315$	(cm^3/sec)	12.6
$V_{in} \pm 0.86$	(cm/sec)	30.0
$\overline{V}_{1\ max} \pm 0.002$	(cm/sec)	0.05
$\rho_{in} \pm 0.0005$	(gr/cm^3)	1.0070
$\nu \pm 3x10^{-6}$	$(cm^2/sec$	$1.2x10^{-2}$
$D \pm 0.1$	(cm)	45
$h_L \pm 0.5$	(cm)	23

viscosity measurements, respectively, but after examining the variation of temperature within the model reservoir (Figure 26) and the difference between reservoir temperatures and calibration temperatures, it was concluded that temperature was negligible in controlling densities. It was also determined that the concentrations of salt solution used had a very minor effect of viscosity.

In the measurements of the reservoir current by means of dye profiles, the steps involved the projection of slides into a viewer cabinet. In doing so, the various images were first aligned with reference bolts on the front side of the reservoir tank in order to match the scale on the viewer cabinet. Moreover, the distance in from the wall to various dye streaks was slightly

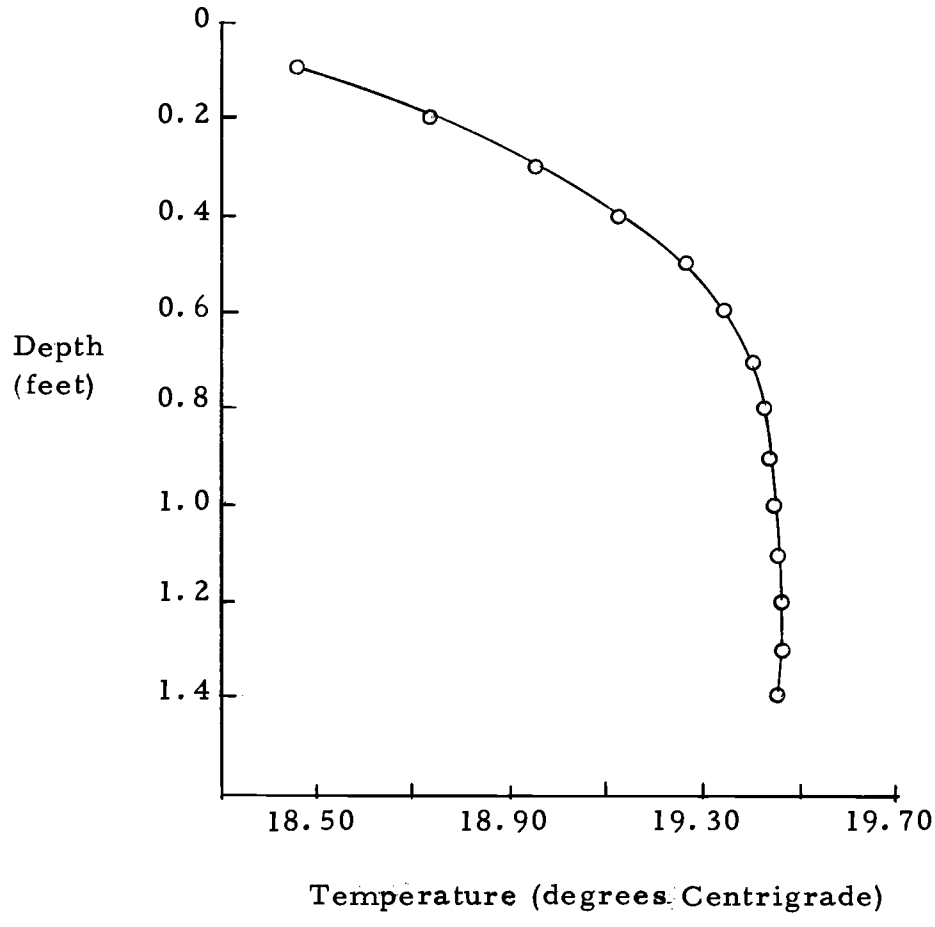

Figure 26. Initial variation of temperature within model reservoir

variable making slight parallax errors in the photographically determined lengths. Thus, possibly the largest inherent error in taking any measurement occurred in the determination of the reservoir current velocities.

It is believed that the propagation of the above tolerance in computing the parameters plotted in Chapter IV are the cause of much of the scatter shown in Figures 18 through 24.

2. Limitations of the Investigation

Certain assumptions necessary to simplify the analysis in this model study imposed limitations on the results obtained. The streamflow rate, Q_{in}, definitely varies with time in a prototype situation and would be expected to have a large effect in reservoir density current flows. In this study the streamflow rate was held constant. It was seen in the discussion of thermal stratification that the density gradient varies with time and usually also changes with depth. The density gradient was also made constant. The effects of holding the streamflow rate and density gradient constant limits the results considerably. The existence of the h_{in} variable is also limiting in that h_{in}'s meaning should be questioned. Figure 27 shows cross sections of the model configuration and an idealized reservoir.

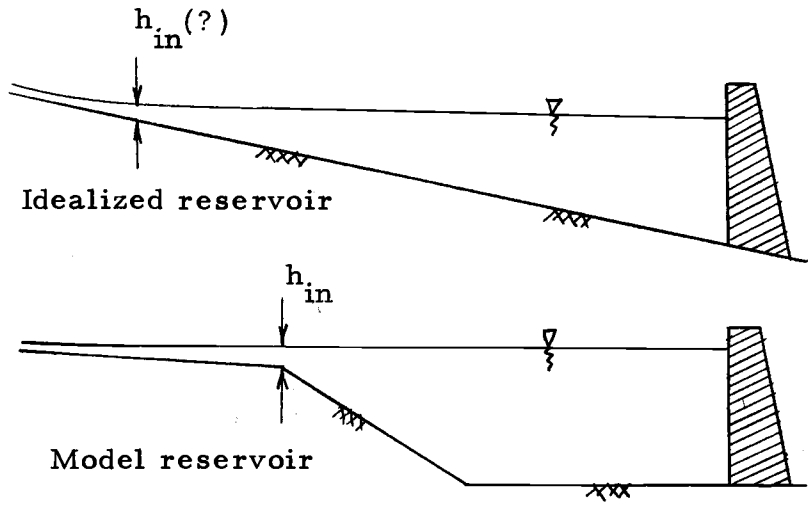

Figure 27. Configuration of an idealized reservoir and the model reservoir.

In the model reservoir a double slope configuration is necessary to insure correctly scaled streamflow velocities while at the same time providing adequate depth in the model reservoir. The depth of water at the intersection of the two slopes is defined as h_{in}. An idealized reservoir is usually described with the bottom of the reservoir and the streambed as one slope, and h_{in} is not really defined, although in some cases sediment may alter the configuration, creating a type of h_{in} parameter.

Time influenced the behavior of the model reservoir currents in many ways. As the inflow currents approached the outlet of the tank, their speed of advancement slowed down due to a blocking phenomena, and the inflow current velocities became a function of

time. Secondly, a noticeable shift in the density profile appeared after a period of time due to the combination of withdrawal and inflow in a model reservoir of limited size. Figure 28 shows the density profile both before and after a typical run. Both of these effects were to be disregarded by making two restrictions on the investigation. The experimental data was taken at a reference station which was 10.5 feet from the model stream mouth, and the measurements were not taken beyond the time that blocking has no influence. These restrictions limited the study to be valid only for density flows in the upper reaches of a reservoir. This one reference station also prevented the results from including the effects of variation in x.

Although the flow in the model reservoir was intended to be two-dimensional, variations from two-dimensional flow were observed in the reservoir currents as a meandering from side to side as shown in Figure 29. The meandering presented difficulties in the measurement of the actual reservoir currents because from the side view, the currents appeared to vary in velocity with time. The problem was solved by averaging the photographed current velocities, $V_{i\,max}$, to obtain a net average velocity of advancement, $\bar{V}_{i\,max}$. The meandering phenomena appeared to be a function of the tank geometry and current velocity, and possibly the behavior could be described in terms of a

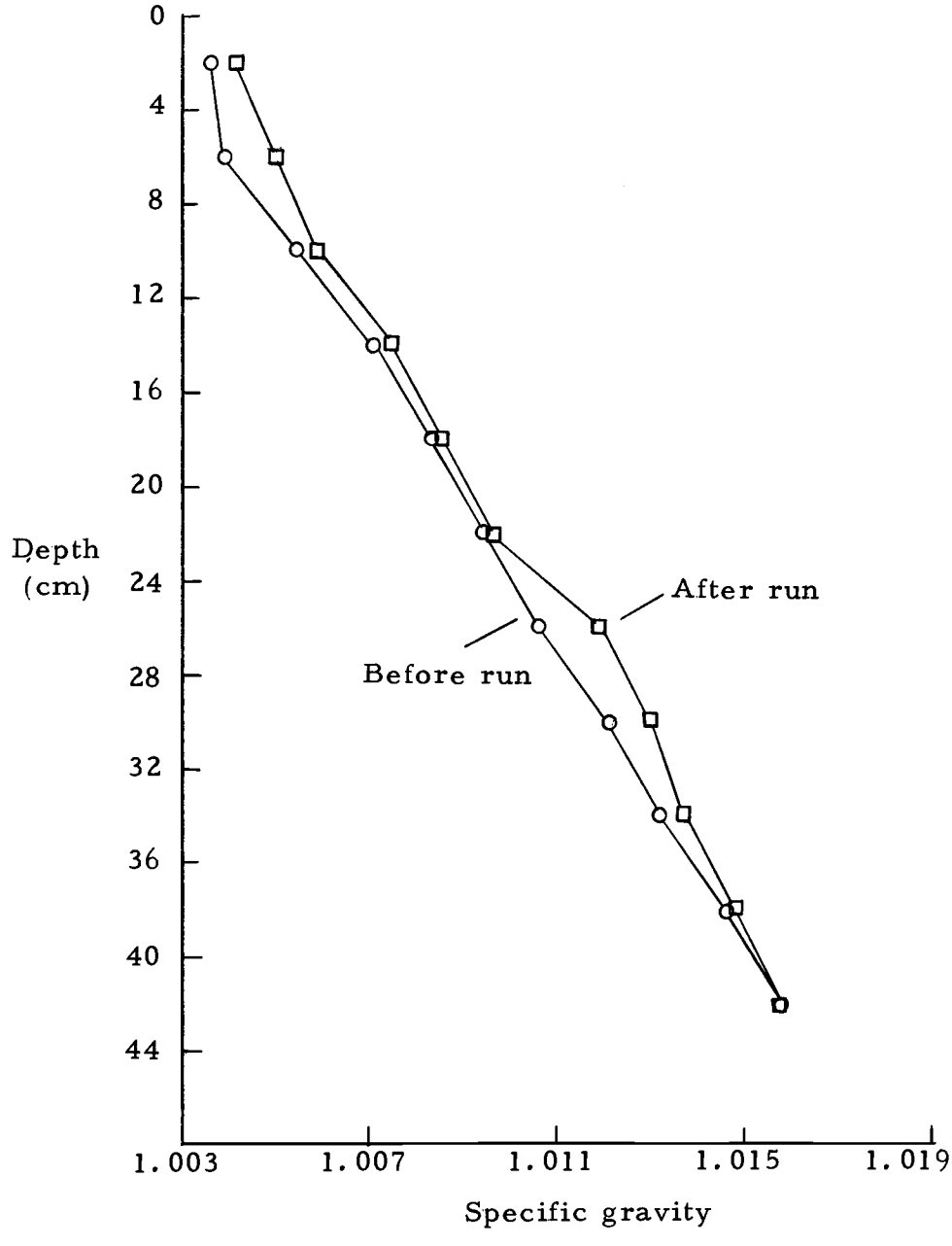

Figure 28. Density profile shift

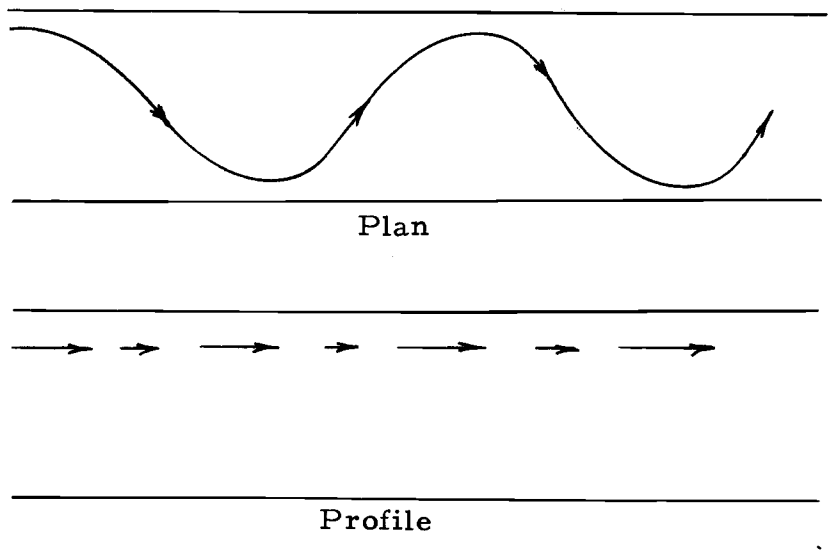

Figure 29. Meandering of Reservoir Currents

Strouhal number or Brunt - Väisälä frequency.

3. Model - Prototype Relationship

The scaling of results obtained from a model study to a prototype is based on the laws of similitude, which require the model and the prototype to be similar, geometrically, kinematically, and dynamically. Geometric similarity implied that all significant geometric parameters, in dimensionless form, are the same for the model and prototype, and kinematic similarity exists when the streamline patterns in the model and the prototype are the same. Dynamic similarity exists when the ratios of forces at corresponding points in the flow have equal values in both model and prototype

and implies both geometric and kinematic similarity.

The requirement for dynamic similar fluid motions of any incompressible viscous free surface fluid in a gravity field is equality of Froude and equality of Reynolds numbers in both systems. Specifying the equality of the Froude numbers,

$$\frac{Fr_m}{Fr_p} = Fr_r = \frac{V_r}{\sqrt{g_r L_r}} = 1.0$$

or

$$V_r = \sqrt{g_r L_r} .$$

From the equality of Reynolds numbers,

$$V_r = \frac{\mu r}{\rho_r L_r} .$$

Since the velocity ratios must be the same, and since for terrestrial events gr=1,

$$L_r = \left(\frac{\mu r}{\rho r}\right)^{2/3} = \nu^{2/3}.$$

For dynamic similitude of both viscous and gravity effects the choice of fluid determines the length ratio, and since similar fluids are used in the model and the prototype, the criteria cannot be satisfied unless the scale ratio is close to unity. Usually in open channel systems, if the viscous effects are small in comparison to gravity effects, only a Froude number similarity is required.

Using a Froude number scaling criteria and a length ratio, $\frac{L_m}{L_p} = \frac{1}{200}$, Table 2 is formed. Table 2 shows the model-prototype scaling parameters in this investigation.

Table 2. Model-prototype scaling parameters.

	Model	Ratio	Prototype
Reservoir:			
length (ft)	20.0	$Lr=5x10^{-3}$	4000
width (ft)	1.50	$Lr=5x10^{-3}$	300
depth (ft)	1.48	$Lr=5x10^{-3}$	296
surface area (ft^2)	30	$AR=2.5x10^{-5}$	$1.2x10^{6}$
volume (ft^3)	44.4	$V=1.25x10^{-7}$	$3.55x10^{8}$
Stream:			
depth (ft)	0.01	$Lr=5x10^{-3}$	2
width (ft)	0.046	$Lr-5x10^{-3}$	29.2
velocity (ft/sec)	0.1-0.9	$Vr=0.0708$	1.41-12.7
discharge (ft^3/sec)	$4.46x10^{-4}$	$Qr=1.77x10^{-6}$	252

The Froude scaling assumption requires that the model is large enough to ignore viscous effects. In the experimental runs, however, it appeared that the model reservoir currents behaved as laminar flow meaning that viscous effects were significant.

How can laminar flow in a modeling scheme provide insight into flows in a prototype reservoir, which are expected to be turbulent because of the large scale or large Reynolds numbers, and how does a model using a Froude scale criteria compare with the prototype reservoir? Consider the inertia forces and resistance

forces in the form of a Reynolds number with eddy viscosity, E, included in the resistance term.

$$Re^{1} = \frac{\text{inertia}}{\nu+E}$$

Similarity between the laminar model currents and prototype currents should occur if

$$\left(\frac{\text{inertia}}{\nu+E}\right)_{\text{model}} \approx \left(\frac{\text{inertia}}{\nu+E}\right)_{\text{prototype}}$$

Since the model is laminar in behavior the eddy viscosity of the model is assumed to be zero. Similarity will be established if $E_{\text{prototype}}$ can be of an order of magnitude to equalize the ratios.

The turbulent eddy viscosity is difficult to quantitize, but an order of magnitude value may be obtained. Assume that reservoir currents due to entering streamflow are a type of columnar flow somewhat similar to a two-dimensional jet. For two-dimensional jetflow Schlichting (26) has shown that the turbulent eddy viscosity may be expressed as a function of a characteristic velocity, U_{max}, and a length denoting half the width at half depth,

$$E_p = 0.026\ b_{\frac{1}{2}}\ U_{max}.$$

Since it was seen that

$V_m \approx 0.043 \frac{cm}{sec}$; $b_m = 45$ cm; $E_m = 0$; and

$\nu_m = \nu\rho = 1.2 \times 10^{-2}$ cm^2/sec,

the modified Reynolds numbers are:

$$(195)_{model} \approx (78)_{prototype}.$$

The Reynolds analogy hypothesis (29), i.e., the eddy diffusion coefficient for mass transport approximates the eddy viscosity coefficient for momentum transport, may also be assumed. Predictions from lake and reservoir measurements by Bella (3) and Orlob (24) have shown effective diffusion coefficients to range from $0.1 cm^2/sec$ to $10 cm^2/sec$ by assuming a one-dimensional assumption with no velocity profile. Expecting the coefficient to be higher where density flows are involved, $E_m = \frac{10 cm^2}{sec}$, may be substituted into the prototype modified Reynolds number along with the prototype values for velocity and width,

$$(195)_{model} \approx (216)_{prototype}.$$

The two ratios of the same order of magnitude suggests that viscosity in the small scale of the model simulates the eddy viscosity in the actual reservoir allowing laminar flow to give insight to

prototype reservoir flows. The validity of the Froude scaling could be verified by comparing the characteristics of the model study with characteristics of an actual prototype reservoir, but at this time there is insufficient field evidence.

4. Suggestions for Further Study

A natural extension of this experimental work would be to eliminate a number of limiting assumptions by examining the effect of an increased number of interacting independent variables. Important extensions would involve the variation of the streamflow rate and the density gradient. It would be also important to examine the variation of various factors with the length of the tank and time. An important aspect involving length of the reservoir and time is the blocking effect and meandering. Specifically when and where does blocking occur?

Another phenomena which merits more study is the reinforcing effect between inflowing density currents and withdrawal currents. This phenomenon appears significant in the control of reservoir detention time.

Field data for reservoir density currents is insufficient. Field studies are needed for the verification of laboratory scaling criteria and a greater understanding of the behavior of flow patterns.

VI. SUMMARY AND CONCLUSIONS

An experimental study of entering streamflow effects on currents of a density stratified model reservoir was made. The major conclusions will be summarized as follows:

1. For the range of values tested the entering model streamflow created two possible main inflow density currents in the model reservoir.

2. The upper inflow current increased its magnitude and the lower inflow current decreased its magnitude as the model streamflow Reynolds number increased. For the range of streamflow parameters tested these currents could be described by the following relationships:

$$\bar{V}_{1\,max} = \frac{\nu_{res}}{b}\left[-0.5\,\mathrm{Log}\left[\left(\frac{V_{in}b_{in}}{\nu_{in}}\right)\left(\frac{D}{D-h_1}\right)\right] + 365\right],$$

$$\bar{V}_{3\,max} = \left[\left(\frac{\rho_{max}-\rho_o}{\rho_{max}}\right) h_3\, g\right]^{1/2}\left[1.67\times10^{-4}\,\frac{V_{in}b_{in}}{\nu_{in}} + 0.42\right].$$

3. The lower inflow current will no longer occur at a model streamflow number greater than

$$\frac{V_{in}b_{in}}{\nu_{in}} = 1.66\times10^{5}\left(\frac{D-h_1}{D}\right).$$

4. The elevation of the upper inflow current was independent

of V_{in} and ρ_{in}. The elevation of the lower inflow current was dependent on ρ_{in} and the mixing which occurred at the stream mouth.

5. The interaction between two reservoir density currents created a significant reinforcement of both currents.

6. The blocking effect due to reservoir stratification and the influence of geometry may have significant influence on internal model reservoir currents created by entering model streamflow.

7. A reservoir model with laminar behavior probably gives much insight to problems associated with flow in prototype reservoirs.

BIBLIOGRAPHY

1. Abraham, G. Horizontal jets in stagnant fluid of other density. Proceedings of the American Society of Civil Engineers, Journal of the Hydraulics Engineering Division 91:138-154. 1965.

2. Bell, H. G. Stratified flow in reservoirs and its use in the prevention of silting. Washington, D. C., 1942, 65 p. (U. S. Department of Agriculture. Miscellaneous Publication no. 491)

3. Bella, D. A. The effects of sinking and vertical mixing on algal populations in lakes and reservoirs. (Unpublished research. Corvallis, Oregon State University, Department of Civil Engineering, 1969.

4. Brooks, N. H. and R. C. Koh. Selective withdrawal from density-stratified reservoirs. Pasadena, 1968. 46 p. (California Institute of Technology. W. M. Keck Laboratory of Hydraulics and Water Resources. Report no. KH-P-66)

5. Brush, L. M., F. C. McMichael and Chin Y. Kuo. Artificial mixing of density-stratified fluids: a laboratory investigation. Princeton, 1968. 80 p. (Princeton University. Lewis F. Moody Hydrodynamics Laboratory. Report no. MH-R-2)

6. Churchill, M. A. Effects of storage impoundments on water quality. Transactions of the American Society of Civil Engineers 123:419-464. 1958.

7. Clay, C. H. and R. A. Fahlman. The Big Qualicum River fisheries development project. (Reprint from: The B. C. Professional Engineer. December, 1962)

8. Daily, J. W. and D. R. F. Harleman. Fluid dynamics. Reading, Massachusetts, Addison-Wesley, 1966. 454 p.

9. Dake, J. M. K. and D. R. F. Harleman. An analytical and experimental investigation of thermal stratification in lakes and ponds. Cambridge, 1966. 271 p. (Massachusetts Institute of Technology. Department of Civil Engineering. Report no. 99)

10. Debler, Walter R. Stratified flow into a line sink. Proceedings of the American Society of Civil Engineers, Journal of the Engineering Mechanics Division 85(3): 51-65. 1969.

11. Ellison, T. H. and J. S. Turner. Turbulent entrainment in stratified flows. Proceedings of the American Society of Civil Engineers, Journal of Fluid Mechanics 6:423-448. 1959.

12. Fan, L. N. Turbulent buoyant jets into stratified or flowing ambient fluids. Pasadena, 1967. 196 p. (California Institute of Technology. W. M. Keck Laboratory of Hydraulics and Water Resources. Report no. KH-R-i5)

13. Fietz, T. R. The measurement of characteristics of a three dimensional density current. Manly Vale, Australia, 1966. 193 p. (The University of New South Wales. Water Research Laboratory. Report no. 85)

14. Fry, A. S., A. Churchill and Rex A. Elder. Significant effects of density currents in TVA's integrated reservoir and river system. In: Proceedings of the Minnesota International Hydraulics Convention, Minneapolis, 1953. Dubuque, Iowa, W. M. C. Brown, 1953. p. 335-354.

15. Kao, T. W. A free streamline solution for stratified flow into a line sink. Journal of Fluid Mechanics 21:535-543. 1965.

17. Koh, R. C. Y. Viscous stratified flow towards a line sink. Pasadena, 1964. 172 p. (California Institute of Technology. W. M. Keck Laboratory of Hydraulics and Water Resources. Report no. KH-R-6)

18. Lofquist, K. Flow and stress near an interface between stratified fluids. Physics of Fluids 3:158-175. 1960.

19. Long, Robert R. Some aspects of the flow of stratified bluids. I. Tellus 5:42-58. 1953.

20. Long, Robert R. Some aspects of the flow of stratified fluids. III. Tellus 7:342-357. 1955.

21. Middleton, G. V. Experiments of density and turbidity currents. Canadian Journal of Earth Sciences 3:627-636. 1966.

22. Morton, B. R. On a momentum-mass flux diagram for turbulent jets, plumes and wakes. Proceedings of the American Society of Civil Engineers, Journal of Fluid Mechanics 10:191-112. 1961.

23. Morton, B. R., G. I. Taylor and J. S. Turner. Turbulent gravitational convection from maintained and instantaneous sources. Proceedings of the Royal Society (London), ser. A, 234:1-23.

24. Orlob, J. Prediction of thermal energy distribution in streams and reservoirs. Walnut Creek, California, Water Resource Engineering, Incorporated, 1967. 18 p. (Prepared for California Department of Fish and Game)

25. Ross, R. L. and N. J. MacDonald. The effect of Libby Reservoir, Montana, on water temperatures. In: Proceedings of the Hydraulics Division of the 16th Annual Specialty Conference, Massachusetts Institute of Technology, Cambridge, Massachusetts, 1968. p. 1-14.

26. Rumer, R. R. Longitudinal dispersion in steady and unsteady flow. Proceedings of the American Society of Civil Engineers, Journal of the Hydraulics Engineering Division 88:147-172. 1962.

27. Schlichting, H. Boundary-layer theory. 6th ed. New York, McGraw-Hill, 1968. 747 p.

28. Spurkland, T. The effects of boundary geometry on internal density currents in a density stratified reservoir. Master's thesis. Corvallis, Oregon State University, 1968. 44 numb. leaves.

29. Townsend, A. A. Turbulence. In: Handbook of fluid dynamics, ed. by V. L. Streeter. New York, McGraw-Hill, 1961. p. 10-18.

30. Wada, A. Numerical analysis of distribution of flow and thermal diffusion caused by outfall of cooling water. Tokyo, 1969. 23 p. (Central Research Institute of Electric Power

Industry. Technical Laboratory. Report no. 67004)

31. Yih, C. S. On the flow of a stratified fluid. In: Proceedings of the Third U.S. Congress of Applied Mechanics, Providence, R.I., 1958. New York, American Society of Mechanical Engineers, 1958. p. 857-861.

APPENDICES

APPENDIX A. Summary of Notations.

For simplicity, symbols of secondary importance which are defined in the text are omitted from the following list:

C	Concentration of solute in the stratified fluid
D	Depth of model reservoir
D'	Diffusion coefficient
$\frac{d\rho}{dy}$	Density gradient
E_l	Turbulent eddy coefficient
Fr	Froude number
g	gravitational acceleration
h_l	Depth from free surface
h_{in}	Depth of change in slope
k	Coefficient of entrainment
P	Pressure
Q_l	General current designation
Re	Modified Reynolds number including a turbulent eddy coefficient
S_v	Slope of streambed
S_r	Slope of upper reservoir floor
s'	Rectangular coordinate in direction of streambed
t	Time
t'	Rectangular coordinate normal to s' vertically

APPENDIX A (continued)

T_l	Temperature
u	Velocity component in x-direction
$u(s', t', v')$	Lagrangian velocity in s-direction
v	Velocity component in y-direction
v'	Rectangular coordinate normal to s' and t'
$V_{l\ max}$	Maximum instantaneous velocity of various reservoir currents
$\overline{V}_{l\ max}$	Maximum average velocity of various reservoir currents
x	Horizontal rectangular coordinate
y	Vertical rectangular coordinate
γ_l	Specific weight
θ	Angle of upper reservoir slope
μ	Kinematic viscosity
ν_l	Dynamic viscosity
ρ_l	Density
$\rho_l(s', v', t')$	Lagrangian density with respect to s, v, t
τ_l	Shearing stress
ϕ	Angle of streambed
ψ	Streamfunction
∇	Gradient operator

APPENDIX A. (continued)

Subscripts

a	Ambient fluid
l	General subscript
in	Inflowing fluid
m	Model
max	Maximum
out	Outflow
p	Prototype
res	Reservoir

APPENDIX B. Values of Physical Constants

D	cm.	45
b_{in}	cm.	4.45
b	cm.	45.7
L	cm.	580.
d_o	cm.	0.952
h_o	cm.	23.0
θ	degrees	9.2
ρ_o	gr/cm^3	1.001
Q_{in}	cm^3/sec	12.6
Q_o	cm^3/sec	12.6
h_{in}	cm.	1.27
g	cm/sec^2	980
ρ_{max}	gr/cm^3	1.017

APPENDIX C. Summary of Data

Test	11	12	13	14	15	16	17
S_v	0.0052	0.0070	0.0070	0.0052	0.0096	0.0096	0.0096
V_{in} (cm/sec)	5.45	6.37	7.28	5.85	8.32	7.47	8.38
ρ_{in} (gr/cm^3)	1.0155	1.0123	1.0087	1.0054	1.0155	1.0120	1.0083
$\frac{\Delta\rho}{\Delta y}$ (gr/cm^4)x10^4	3.13	3.25	2.95	3.16	3.31	3.13	3.24
d_{in} (cm)	0.518	0.445	0.388	0.484	0.340	0.379	0.338
T_{in} (^{o}C)	13.0	12.5	13.0	12.5	12.5	13.5	12.5
ν_{in} (cm^2/sec)x10^2	1.213	1.227	1.213	1.227	1.227	1.199	1.227
$\bar{V}_{1\ max}$(cm/sec)x10^2	4.07	8.48	5.93	6.57	3.81	5.60	5.80
$\bar{V}_{2\ max}$(cm/sec)x10^2	5.72	8.48	6.00	5.21	5.68	5.25	5.34
$\bar{V}_{3\ max}$(cm/sec)x10^2	4.49	4.74	4.66	4.66	4.87	4.75	4.53
h_1 (cm)	38.0	24.5	19.5	10.5	37.0	26.5	18.0

APPENDIX C. (continued)

Test	11	12	13	14	15	16	17
h_2 (cm)	23.0	23.5	23.0	23.0	23.0	23.0	23.0
h_3 (cm)	6.0	7.0	6.0	6.0	6.5	6.5	6.0
T_{res} (^{o}C)	17.0	17.5	16.5	17.0	17.0	17.5	17.0
ν_{res} (cm^2/sec)x10^2	1.093	1.079	1.106	1.093	1.093	1.079	1.093
$\frac{\bar{V}_{1\,max}{}^{b}}{\nu_{res}}$	170.5	359.0	245.0	275.0	159.5	231.0	242.7
$\frac{V_{in}{}^{b}{}_{in}}{\nu_{in}}$	2006.0	2311.0	2670.0	2120.0	3010.0	2770.0	3040.0
$\frac{D}{D-h_1}$	6.43	2.20	1.77	1.30	5.62	2.43	1.67
$\frac{h_1}{D}$	0.845	0.545	0.433	0.233	0.822	0.589	0.400
$\frac{h_3}{D}$	0.133	0.155	0.133	0.133	0.144	0.144	0.133

APPENDIX C. (continued)

Test	11	12	13	14	15	16	17
$\frac{h_o - h_1}{D}$	-0.333	-0.033	-.078	0.278	-0.311	-0.078	0.111
$\frac{\bar{V}_{2\,max} d_o^2}{Q_{out}}$	0.411	0.610	0.434	0.375	0.408	0.377	0.384
$\left(\frac{\rho_{in} - \rho_o}{D}\right) \frac{\Delta y}{\Delta \rho}$	1.032	0.772	0.577	0.309	0.977	0.780	0.500
$\frac{V_{3\,max}}{\left[g\left(\frac{\rho_{max} - \rho_o}{\rho_{min}}\right) h_3\right]^{\frac{1}{2}}}$	0.453	0.443	0.470	0.470	0.472	0.460	0.457
$\left(\frac{V_{in} b_{in}}{\nu_{in}}\right) \frac{D}{D-h_1}$	12870.	5080.	4720.	2760.	16900.	6740.	5080.

APPENDIX C. (continued)

Test	18	19	20	21	22	23	24
S_v	0.0096	0.0165	0.0183	0.0165	0.9165	0.0218	0.0209
V_{in} (cm/sec)	8.48	11.19	11.13	13.47	12.20	16.36	13.81
ρ_{in} (gr/cm^3)	1.0054	1.0155	1.0118	1.0087	1.0054	1.0155	1.0120
$\frac{\Delta\rho}{\Delta y}$ (gr/cm^4)x10^4	3.33	3.16	3.13	3.07	3.00	2.96	3.06
d_{in} (cm)	0.334	0.253	0.255	0.210	0.232	0.173	0.206
T_{in} (^{o}C)	13.0	12.5	13.0	13.0	12.0	11.0	11.5
ν_{in} (cm^2/sec)x10^2	1.213	1.227	1.213	1.213	1.242	1.270	1.256
$\bar{V}_{1\ max}$ (cm/sec)x10^2	6.40	3.56	5.21	5.20	6.23	3.18	4.66
$\bar{V}_{2\ max}$(cm/sec)x10^2	5.38	5.38	6.10	4.36	4.95	5.34	5.08
$\bar{V}_{3\ max}$(cm/sec)x10^2	4.49	4.87	5.26	5.34	5.00	5.72	5.04
h_1 (cm)	10.5	37.5	26.0	20.5	9.5	37.0	29.0

APPENDIX C. (continued)

Test	18	19	20	21	22	23	24
T_{res} (^{o}C)	17.0	17.5	17.0	16.5	16.0	14.5	14.0
ν_{res} (cm^2/sec)x10^2	1.093	1.079	1.093	1.106	1.120	1.165	1.181
$\frac{\bar{V}_{l\,max}\,b}{\nu_{res}}$	267.8	151.0	218.1	220.9	254.2	124.8	180.5
$\frac{V_{in}\,b_{in}}{\nu_{in}}$	3110.0	4050.0	4070.0	4930.0	4360.0	5730.0	4890.0
$\frac{D}{D-h_1}$	1.30	6.00	2.37	1.84	1.27	5.63	2.82
$\frac{h_1}{D}$	0.233	0.834	0.578	0.455	0.211	0.822	0.645
$\frac{h_3}{D}$	0.133	0.144	0.144	0.133	0.155	0.155	0.133
$\frac{h_o-h_1}{D}$	0.278	-0.322	-0.067	0.056	0.300	-0.311	-0.133

APPENDIX C. (continued)

Test	18	19	20	21	22	23	24
$\frac{\bar{V}_{2\,max} d_o^2}{Q_{out}}$	0.387	0.387	0.439	0.313	0.356	0.384	0.365
$\frac{\rho_{in} - \rho_o}{D} \frac{\Delta y}{\Delta \rho}$	0.294	1.021	0.767	0.557	0.326	1.090	0.799
$\frac{\bar{V}_{3\,max}}{\left[g\left(\frac{\rho_{max} - \rho_0}{\rho_{max}}\right) h_3\right]^{\frac{1}{2}}}$	0.452	0.472	0.510	0.525	0.468	0.534	0.509
$\left(\frac{V_{in} b_{in}}{\nu_{in}}\right) \frac{D}{D-h_1}$	4040.	24, 300.	9660.	9070.	5540.	32, 210.	12, 800.

APPENDIX C. (continued)

Test	25	26	27	28	29	30
S_v	0.0326	0.0387	0.0383	0.0409	0.0387	0.0622
V_{in} (cm/sec)	20.28	21.10	23.03	23.52	22.70	28.83
ρ_{in} (gr/cm^3)	1.0155	1.0155	1.0120	1.0089	1.0050	1.0151
$\frac{\Delta\rho}{\Delta y}$ (gr/cm^4)x10^4	3.16	3.13	3.00	3.06	3.13	3.18
d_{in} (cm)	0.140	0.134	0.123	0.120	0.125	0.098
T_{in} (^oC)	12.0	12.0	12.0	12.5	12.0	13.0
ν_{in}(cm^2/sec)x10^2	1.242	1.242	1.242	1.227	1.242	1.213
$\bar{v}_{1\ max}$ (cm/sec)x10^2	2.80	2.54	3.39	1.53	10.21	1.70
$\bar{V}_{2\ max}$(cm/sec)x10^2	4.91	5.59	6.35	4.91	5.04	5.34
$\bar{V}_{3\ max}$(cm/sec)x10^2	5.72	5.84	6.14	6.18	10.21	6.42

APPENDIX C. (continued)

Test	25	26	27	28	29	30
h_1 (cm)	35.0	37.0	28.5	13.5	7.5	37.0
h_2 (cm)	23.0	23.0	24.0	23.0	23.0	23.5
h_3(cm)	7.0	7.0	7.5	7.5	7.5	7.0
T_{res} (^{o}C)	16.0	16.0	16.0	16.0	16.5	16.0
ν_{res}(cm^2/sec)	1.120	1.120	1.120	1.120	1.106	1.120
$\frac{V_{l\,max}{}^{b}}{\nu_{res}}$	114.3	103.7	138.4	185.0	422.0	69.4
$\frac{V_{in}{}^{b}{}_{in}}{in}$	7260.0	755.0	8250.0	8530.0	8130.0	10,580.0
$\frac{D}{D-h_1}$	4.50	5.63	2.72	1.43	1.20	5.63
$\frac{h_1}{D}$	0.778	0.822	0.634	0.300	0.167	0.822

APPENDIX C. (continued)

Test	25	26	27	28	29	30
$\frac{h_3}{D}$	0.155	0.155	0.166	0.166	0.166	0.155
$\frac{h_1 - h_2}{D}$	-0.266	-0.311	-0.122	0.211	0.344	-0.311
$\frac{\bar{V}_{2\,max} d_o^2}{Q_{out}}$	0.353	0.402	0.457	0.353	0.362	0.384
$\frac{\rho_{in} - \rho_o}{D} \frac{\Delta y}{\Delta \rho}$	1.029	1.033	0.814	0.572	0.283	0.986
$\frac{\bar{V}_{3\,max}}{\left[g\left(\frac{\rho_{max} - \rho_o}{\rho_{max}}\right) h_3\right]^{\frac{1}{2}}}$	0.534	0.546	0.554	0.554	0.921	0.600
$\left(\frac{V_{in} b_{in}}{\nu_{in}}\right) \frac{D}{D-h_1}$	32,600.	42,500.	22,400	12,200	9750.	59,600.